the nucleus (Fig. 2D), suggesting that the L377A/L384A mutations had destroyed the functional NES (amino acid residues L377–L384) of NORE1A. Next, we transfected H1299 cells with the one of the GFP-NORE1A plasmids or control GFP expression plasmid and exposed them to HU for 40 h. Determination of centrosome number in these cells after immunofluorescence analysis with anti-γ-tubulin antibody revealed that two of mutants, NORE1A-L290A/I292A and -L344A/L346A, as well as NORE1A-wt had activity that significantly suppressed the centrosome amplification induced by HU, but that the NORE1A-L377A/L384A mutant did not possess such activity (Fig. 2E). These observations provided further evidence for activity of centrosomal NORE1A that regulates the centrosome number in cells exposed to HU.

3.5. *NORE1A suppresses CIN in HU-treated cells*

Next, we attempted to determine whether the activity of NORE1A that suppresses the centrosome amplification in HU-exposed H1299 cells is translated into a difference in the level of chromosome destabilization as assessed by FISH analysis. H1299 cells were transfected with GFP, GFP-NORE1A-wt, or GFP-NORE1A-L377A/L384A (NES mutant) plasmid together with a plasmid containing a puromycin resistance gene, and after puromycin selection, the cells were exposed to HU for 40 h. After washing, the cells were then cultured for an additional 72 h, and subjected to FISH analysis with probes specific for chromosomes 2 and 16. When the cells were divided according to number of chromosomes per cell into cells containing the modal chromosome number and cells containing other chromosome numbers, cells containing the modal chromosome number were found to be significantly less frequent among the HU-exposed cells than among the control cells (Fig. 3A; Fig. 3B shows representative images). Importantly, comparison of the frequency of cells containing the modal chromosome number among HU-exposed cells showed that it was significantly higher among the cells transfected with the GFP-NORE1A-wt expression vector, but not with the GFP-NORE1A-L377A/L384A expression vector, than among cells transfected with the GFP vector (Fig. 3A and B), suggesting that wt NORE1A, but not NES-mutant NORE1A, suppresses CIN in HU-exposed H1299 cells.

3.6. *Down-regulation of NORE1A mRNA expression in primary NSCLC*

Next, to better understand the status of NORE1A expression in NSCLC, we investigated whether NORE1A expression is also down-regulated in primary NSCLC. NORE1A mRNA expression in 51 primary NSCLC and corresponding non-cancerous lung tissues was measured by QRT-PCR, and the ratio of the level of NORE1A mRNA expression in the cancerous tissue to the level in the corresponding non-cancerous tissue (T/N ratio) was calculated in each case. Reduced NORE1A expression (T/N ratio < 0.5) was observed in 25 of the 51 (49%) primary NSCLC cancers (Fig. 4A). Moreover, a significant difference was detected in the NORE1A expression level between cancerous tissue and the corresponding non-cancerous tissue by a statistical analysis (p-value = 0.013 by Wilcoxon matched pairs test). Reduced NORE1A protein expression in the cancerous tissue compared with the corresponding non-cancerous tissue was detected in two cases showing reduced NORE1A mRNA expression by Western blot analysis (Fig. 4B). These results suggest that NORE1A mRNA expression is down-regulated in primary NSCLCs. Finally, we investigated whether the levels of NORE1A mRNA expression were associated with clinicopathological features in NSCLC patients. Although no associations were found between the clinicopathological factors onset age, smoking history, tumor stage, or tumor histology and the NORE1A mRNA expression levels, the frequency of male patients was higher in the group of NSCLC patients with a T/N ratio < 1 than in the group with a T/N ratio ≥ 1 (p-value = 0.006) (Table 1).

4. Discussion

The results of this study showed that exposure of H1299 NSCLC cells to HU resulted in abnormal centrosome amplification and that forced expression of NORE1A partially suppressed the centrosome amplification. NORE1A-L377A/L384A, an NES mutant form, did not localize to centrosomes and did not suppress the centrosome amplification induced by HU. Furthermore, the results of a FISH analysis showed that wt NORE1A, but not NES-mutant NORE1A, suppressed CIN in HU-exposed H1299 cells. Next, we compared level of NORE1A mRNA expression in the cancerous tissue of primary NSCLCs and corresponding non-cancerous lung tissue by QRT-PCR analysis, and the results showed that NORE1A mRNA expression was down-regulated in 25 (49%) of the 51 primary NSCLCs. These results suggest that NORE1A has activity that suppresses centrosome amplification induced by HU, and they suggested that down-regulation of NORE1A mRNA is one of the common gene abnormalities in NSCLCs.

This study revealed a novel activity of NORE1A that suppresses centrosome amplification induced by HU. Numerical and functional abnormalities of centrosomes result in aberrant mitotic spindle formation, merotelic kinetochore-microtubule attachment errors, lagging chromosome formation, and chromosome segregation errors, all of which are thought to be possible causes of CIN [12–15]. Many cancer-associated proteins have already been reported to be involved in controlling the numerical integrity of centrosomes, centrosome duplication, and centrosome function/behavior [13]. Interestingly, most such cancer-associated proteins are localized at centrosomes [12,13]. For example, tumor suppressor p53 is involved in the control of numerical integrity of centrosomes [13,18,30,32]. The p53 is a nucleocytoplasmic shuttling protein and some p53 is localized at centrosomes [13,18,30,32–34]. We therefore think that it is reasonable to conclude NORE1A, some of which is localized at centrosomes, has activity that controls the numerical integrity of centrosomes. However, it is unknown how NORE1A suppresses the centrosome amplification in HU-exposed cells. Since HU is a DNA synthesis inhibitor, cells exposed to HU become arrested in the S-phase of the cell cycle. Centrosomes continue to reduplicate in the absence of DNA synthesis, which is effectively observed if *p53* is lost or mutated [13,16–20,30,32]. Thus, it is speculated that NORE1A has some influence on centrosome reduplication in HU-arrested cells. Future investigation of the mechanism underlying the phenomenon should improve our understanding of carcinogenesis in the lung.

We constructed three NORE1A expression plasmids, each of which contains mutations in the NES region predicted by NetNES server [31], but only the NORE1A-L377A/L384A expression plasmid failed to exhibit cytoplasmic localization, suggesting that the leucine-rich amino acid residues L377–L384 (LQNFLTIL) of NORE1A are a functional NES. Park et al. also showed that this NES sequence is functional [8]. Interestingly, comparison of the amino acid sequences of NORE1A orthologues has shown that the NES region is conserved among *Homo sapiens*, *Mus musculus*, *Rattus norvegicus*, and *Bos taurus*. Since the cytoplasmic localization of NORE1A is essential for its growth-suppressive activity [6] and abrogation of nuclear export results in failure to suppress centrosome amplification as shown in this study, the NES sequence of NORE1A must be important in achieving these functions.

The FISH analysis (Fig. 3) of HU-exposed cells in our study showed a significantly higher proportion of cells containing the modal chromosome number among the cells transfected with the

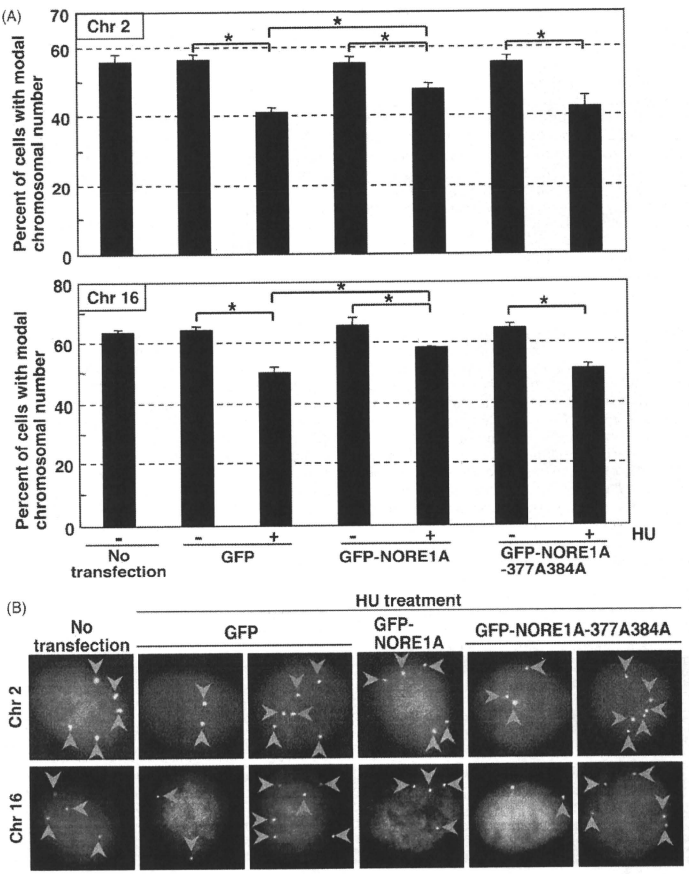

Fig. 3. Wild-type (wt) NORE1A, but not nuclear export signal (NES)-mutant NORE1A, suppresses chromosome instability in hydroxyurea (HU)-exposed H1299 cells. (A and B) H1299 cells were transiently transfected with GFP, GFP-NORE1A-wt, or GFP-NORE1A-L377A/L384A plasmid together with a plasmid containing a puromycin resistance gene, and 40 h later, the cells were exposed to HU for 40 h. The cells were then replated in fresh medium, cultured for an additional 72 h, and subjected to FISH analysis with a Spectrum Orange-labeled centromere enumeration probe. Nuclei were stained with DAPI (blue). The percentages of cells containing the modal chromosome number are shown in the upper panel (chromosome 2) and the lower panel (chromosome 16) of (A). A *t*-test was performed for statistical analysis and an asterisk in the graph indicates a statistically significant difference. Representative images of the results of the FISH analysis are shown in (B). Arrows point to the chromosomes.

GFP-NORE1A-wt expression vector than among the cells transfected with the GFP vector, however, the increase was modest. The fact that the increase was modest is thought to have been due to one of the following possible limitations of this study: (1) HU was not able to induce CIN effectively under the conditions used in our experiment, (2) the use of transiently transfected cells, not stably transfected cells, (3) the H1299 cell line was unsuitable for detecting a clear inhibitory effect of NORE1A on CIN, and (4) chromosomes 2 and 16 were unsuitable for detecting a clear inhibitory effect of NORE1A on CIN.

The cell proliferation analysis in our study revealed that NORE1A has a slight effect on growth suppression in H1299 cells growing as a monolayer on plastic. Two studies on the growth-suppressive function of NORE1A in NSCLC cell lines have been reported [5,6]. In the study by Moshnikova et al. [6] forced expression of NORE1A was found to inhibit anchorage-independent growth of A549 NSCLC cells, but not to affect anchorage-dependent growth of the cells. Aoyama et al. [5] also reported finding that forced expression of NORE1A markedly suppressed anchorage-independent growth of A549 cells, however, they found that under

Table 1
Clinicopathological factors of NSCLC patients according to the T/N ratio of the NORE1A mRNA expression in their lung.

Factor	Total (n = 51)	T/N ≥ 1 (n = 18)	T/N < 1 (n = 33)	p-Value
Age (51 cases)				
Mean ± SD[a]	65.1 ± 12.8 (n = 51)	63.4 ± 13.9 (n = 18)	66.1 ± 12.3 (n = 33)	0.491[b]
Gender (51 cases)				
Male	30(60.1%)	6(33.3%)	24(72.7%)	0.006[c]
Female	21(39.9%)	12(66.7%)	9(27.3%)	
Smoking history (40 cases)				
Smoker	29(65.2%)	7(63.6%)	22(75.9%)	0.447[c]
Non-smoker	11(34.8%)	4(36.4%)	7(24.1%)	
Brinkman index (mean ± SD)	872 ± 1034 (n = 40)	889 ± 973 (n = 11)	866 ± 1072 (n = 29)	0.952[b]
Tumor stage (51 cases)				
I	36(70.6%)	10(55.6%)	26(78.8%)	0.311[c]
II	7(13.7%)	4(22.2%)	3(9.1%)	
III	5(9.8%)	2(11.1%)	3(9.1%)	
IV	3(5.9%)	2(11.1%)	1(3.0%)	
Histology (51 cases)				
Adenocarcinoma	34(66.7%)	10(55.6%)	24(72.7%)	0.231[c]
Squamous cell carcinoma	15(29.4%)	7(38.9%)	8(24.2%)	
Large cell carcinoma	1(2.0%)	0(0.0%)	1(3.0%)	
Adenosquamous carcinoma	1(2.0%)	1(5.6%)	0(0.0%)	

[a] SD, standard deviation.
[b] A t-test was performed.
[c] A chi-square test was performed.

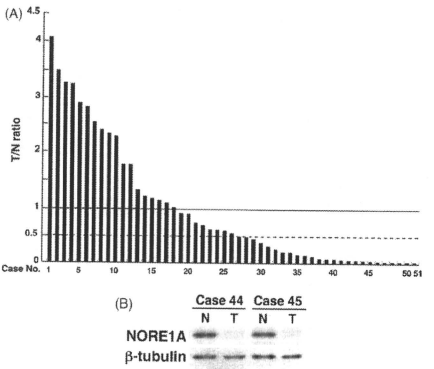

Fig. 4. Down-regulation of NORE1A expression in primary non-small cell lung carcinoma (NSCLC). (A) Down-regulation of NORE1A mRNA expression in primary NSCLC. Comparison between the NORE1A mRNA level in cancerous tissue of 51 primary NSCLCs and corresponding non-cancerous lung tissue as determined by quantitative real-time-polymerase chain reaction analysis. After normalizing the amounts of NORE1A transcripts to those of the GAPD transcript, T/N values were calculated by dividing the amount of normalized transcripts in cancerous tissue by the amount in the corresponding non-cancerous tissue. Differences between the normalized NORE1A mRNA level in cancerous tissue and corresponding non-cancerous tissue were statistically analyzed by the Wilcoxon matched pairs test, and the p-value was 0.013. (B) Down-regulation of NORE1A protein expression in primary NSCLC. Measurement of the level of NORE1A protein expression in cancerous tissue (T) and corresponding non-cancerous tissue (N) by Western blot analysis with anti-NORE1A monoclonal antibody in two NSCLC cases. Expression of β-tubulin protein was analyzed as an internal control.

anchorage-dependent growth conditions NORE1A expression suppressed colony formation by A549 and H460 NSCLC cells by 73% and 23%, respectively. Thus, the growth-suppressive effect of NORE1A under anchorage-dependent conditions seems to be weaker than under anchorage-independent conditions and may vary with the cell type and experimental conditions.

The QRT-PCR analysis in our study revealed that NORE1A mRNA expression was down-regulated in 49% of the primary NSCLCs (n = 51) and in 100% of the NSCLC cell lines (n = 12). The frequency of NORE1A mRNA down-regulation in primary NSCLCs of 49% found in this study is much higher than the frequencies of NORE1A promoter hypermethylation in primary NSCLCs of 24% [22] and 28% [23] reported in the literature. The differences in frequency may be due to the existence of other mechanisms underlying the reduction of mRNA expression level, such as histone deacetylation, microRNA abnormalities, and allelic imbalance [24–26,35]. The results of the expression analysis in this study also showed an association between male NSCLC patients and a reduction of NORE1A expression in the cancerous tissue (T/N ratio < 1). Although the reason for this association is unknown, there are sex differences in the expression of other genes [36,37]. In any event, the results of the mRNA expression analysis suggested that down-regulation of NORE1A mRNA is a common abnormality in the carcinogenesis of NSCLC, the same as down-regulation of p16, RASSF1A, and CDH1 expressions [38,39].

In conclusion, our results suggest that NORE1A has activity that suppresses the centrosome amplification induced by HU and that NORE1A mRNA down-regulation is one of the common gene abnormalities in NSCLCs. These imply a key preventive role of NORE1A against the carcinogenesis of NSCLC.

Conflicts of interest

None declared.

Acknowledgements

We are grateful to Dr. A.V. Khokhlatchev (University of Virginia Health Science Center, VA) for providing us with pCMV5-Flag-NORE1A plasmid vector. We are also grateful to Dr. D.C. Gruenert (California Pacific Medical Center Research Institute, CA) and Dr. T. Kaneko (Yokohama City University, School of Medicine, Japan) for providing us with 16HBE14o- cell line and to Dr. T. Niki (Jichi

Medical University, Japan) for providing us with 7 lung cancer cell lines. We acknowledge Mr. T. Kamo (Hamamatsu University School of Medicine) for his technical assistance. MG is a Center of Excellence research assistant in Hamamatsu Univ Sch Med. This work was supported by grants from the Ministry of Health, Labour and Welfare (19–19), the Japan Society for the Promotion of Science (19790286), the Ministry of Education, Culture, Sports, Science and Technology (20014007), the 21st Century COE program, and the Smoking Research Foundation.

References

[1] Vavvas D, Li X, Avruch J, Zhang XF. Identification of Nore1 as a potential Ras effector. J Biol Chem 1998;273:5439–42.
[2] Tommasi S, Dammann R, Jin SG, Zhang XF, Avruch J, Pfeifer GP. RASSF3 and NORE1: identification and cloning of two human homologues of the putative tumor suppressor gene RASSF1. Oncogene 2002;21:2713–20.
[3] Nakamura N, Carney JA, Jin L, Kajita S, Pallares J, Zhang H, et al. RASSF1A and NORE1A methylation and BRAFV600E mutations in thyroid tumor. Lab Invest 2005;85:1065–75.
[4] Vos MD, Martinez A, Ellis CA, Vallecorsa T, Clark GJ. The pro-apoptotic Ras effector Nore1 may serve as a Ras-regulated tumor suppressor in the lung. J Biol Chem 2003;278:21938–43.
[5] Aoyama Y, Avruch J, Zhang XF. Nore1 inhibits tumor cell growth independent of Ras or the MST1/2 kinases. Oncogene 2004;23:3426–33.
[6] Moshnikova A, Frye J, Shay JW, Minna JD, Khokhlatchev AV. The growth and tumor suppressor NORE1A is a cytoskeletal protein that suppresses growth by inhibition of the ERK pathway. J Biol Chem 2006;281:8143–52.
[7] Moshnikova A, Kuznetsov S, Khokhlatchev AV. Interaction of the growth and tumour suppressor NORE1A with microtubules is not required for its growth-suppressive function. BMC Res Notes 2008;1:1–7.
[8] Park SJ, Lee D, Choi CY, Ryu SY. Induction of apoptosis by NORE1A in a manner dependent on its nuclear export. Biochem Biophys Res Commun 2008;368:56–61.
[9] Calvisi DF, Donninger H, Vos MD, Birrer MJ, Gordon L, Leaner V, et al. NORE1A tumor suppressor candidate modulates p21CIP1 via p53. Cancer Res 2009;69:4629–37.
[10] Joshi HC. Microtubule organizing centers and gamma-tubulin. Curr Opin Cell Biol 1994;6:54–62.
[11] Oakley BR. Gamma-tubulin. Curr Top Dev Biol 2000;49:27–54.
[12] Nigg EA. Centrosome aberrations: cause or consequence of cancer progression? Nat Rev Cancer 2002;2:815–25.
[13] Fukasawa K. Oncogenes and tumour suppressors take on centrosomes. Nat Rev Cancer 2007;7:911–24.
[14] Lingle WL, Barrett SL, Negron VC, D'Assoro AB, Boeneman K, Liu W, et al. Centrosome amplification drives chromosomal instability in breast tumor development. Proc Natl Acad Sci USA 2002;99:1978–83.
[15] Ganem NJ, Godinho SA, Pellman D. A mechanism linking extra centrosomes to chromosomal instability. Nature 2009;460:278–82.
[16] Balczon R, Bao L, Zimmer WE, Brown K, Zinkowski RP, Brinkley BR. Dissociation of centrosome replication events from cycles of DNA synthesis and mitotic division in hydroxyurea-arrested Chinese hamster ovary cells. J Cell Biol 1995;130:105–15.
[17] Tarapore P, Horn HF, Tokuyama Y, Fukasawa K. Direct regulation of the centrosome duplication cycle by the p53-p21Waf1/Cip1 pathway. Oncogene 2001;20:3173–84.
[18] Shinmura K, Bennett RA, Tarapore P, Fukasawa K. Direct evidence for the role of centrosomally localized p53 in the regulation of centrosome duplication. Oncogene 2007;26:2939–44.
[19] Shinmura K, Iwaizumi M, Igarashi H, Nagura K, Yamada H, Suzuki M, et al. Induction of centrosome amplification and chromosome instability in p53-deficient lung cancer cells exposed to benzo[a]pyrene diol epoxide (B[a]PDE). J Pathol 2008;216:365–74.
[20] Dodson H, Bourke E, Jeffers LJ, Vagnarelli P, Sonoda E, Takeda S, et al. Centrosome amplification induced by DNA damage occurs during a prolonged G2 phase and involves ATM. EMBO J 2004;23:3864–73.
[21] Destro A, Ceresoli GL, Baryshnikova E, Garassino I, Zucali PA, De Vincenzo F, et al. Gene methylation in pleural mesothelioma: correlations with clinicopathological features and patient's follow-up. Lung Cancer 2008;59:369–76.
[22] Hesson L, Dallol A, Minna JD, Maher ER, Latif F. NORE1A, a homologue of RASSF1A tumour suppressor gene is inactivated in human cancers. Oncogene 2003;22:947–54.
[23] Irimia M, Fraga MF, Sanchez-Cespedes M, Esteller M. CpG island promoter hypermethylation of the Ras-effector gene NORE1A occurs in the context of a wild-type K-ras in lung cancer. Oncogene 2004;23:8695–9.
[24] Peinado H, Ballestar E, Esteller M, Cano A. Snail mediates E-cadherin repression by the recruitment of the Sin3A/histone deacetylase 1 (HDAC1)/HDAC2 complex. Mol Cell Biol 2004;24:306–19.
[25] Esteller M. Epigenetics in cancer. N Engl J Med 2008;358:1148–59.
[26] Croce CM. Causes and consequences of microRNA dysregulation in cancer. Nat Rev Genet 2009;10:704–14.
[27] Masuda A, Takahashi T. Chromosome instability in human lung cancers: possible underlying mechanisms and potential consequences in the pathogenesis. Oncogene 2002;21:6884–97.
[28] Cozens AL, Yezzi MJ, Kunzelmann K, Ohrui T, Chin L, Eng K, et al. CFTR expression and chloride secretion in polarized immortal human bronchial epithelial cells. Am J Respir Cell Mol Biol 1994;10:38–47.
[29] Kitayama Y, Igarashi H, Watanabe F, Maruyama Y, Kanamori M, Sugimura H. Nonrandom chromosomal numerical abnormality predicting prognosis of gastric cancer: a retrospective study of 51 cases using pathology archives. Lab Invest 2003;83:1311–20.
[30] Ma Z, Izumi H, Kanai M, Kabuyama Y, Ahn NG, Fukasawa K. Mortalin controls centrosome duplication via modulating centrosomal localization of p53. Oncogene 2006;25:5377–90.
[31] la Cour T, Kiemer L, Mølgaard A, Gupta R, Skriver K, Brunak S. Analysis and prediction of leucine-rich nuclear export signals. Protein Eng Des Sel 2004;17:527–36.
[32] Tarapore P, Fukasawa K. Loss of p53 and centrosome hyperamplification. Oncogene 2002;21:6234–40.
[33] Blair Zajdel ME, Blair GE. The intracellular distribution of the transformation-associated protein p53 in adenovirus-transformed rodent cells. Oncogene 1988;2:579–84.
[34] Brown CR, Doxsey SJ, White E, Welch WJ. Both viral (adenovirus E1B) and cellular (hsp70, p53) components interact with centrosomes. J Cell Physiol 1994;160:47–60.
[35] Toma MI, Grosser M, Herr A, Aust DE, Meye A, Hoefling C, et al. Loss of heterozygosity and copy number abnormality in clear cell renal cell carcinoma discovered by high-density affymetrix 10K single nucleotide polymorphism mapping array. Neoplasia 2008;10:634–42.
[36] Mollerup S, Ryberg D, Hewer A, Phillips DH, Haugen A. Sex differences in lung CYP1A1 expression and DNA adduct levels among lung cancer patients. Cancer Res 1999;59:3317–20.
[37] Merino G, van Herwaarden AE, Wagenaar E, Jonker JW, Schinkel AH. Sex-dependent expression and activity of the ATP-binding cassette transporter breast cancer resistance protein (BCRP/ABCG2) in liver. Mol Pharmacol 2005;67:1765–71.
[38] Yokota J, Kohno T. Molecular footprints of human lung cancer progression. Cancer Sci 2004;95:197–204.
[39] Topaloglu O, Hoque MO, Tokumaru Y, Lee J, Ratovitski E, Sidransky D, et al. Detection of promoter hypermethylation of multiple genes in the tumor and bronchoalveolar lavage of patients with lung cancer. Clin Cancer Res 2004;10:2284–8.

EML4-ALK fusion transcripts in immunohistochemically ALK-positive non-small cell lung carcinomas

KAZUYA SHINMURA[1], SHINJI KAGEYAMA[1], HISAKI IGARASHI[1], TAKAHARU KAMO[1], TAKAHIRO MOCHIZUKI[2], KAZUYA SUZUKI[2], MASAYUKI TANAHASHI[3], HIROSHI NIWA[3], HIROSHI OGAWA[4] and HARUHIKO SUGIMURA[1]

[1]First Department of Pathology, and [2]First Department of Surgery, Hamamatsu University School of Medicine, Hamamatsu 431-3192; [3]Division of Thoracic Surgery, Respiratory Disease Center, and [4]Division of Pathology, Seirei Mikatahara General Hospital, Hamamatsu 433-8558, Japan

Received October 12, 2009; Accepted November 27, 2009

DOI: 10.3892/etm_00000042

Abstract. EML4-ALK fusion transcripts have been found in a subset of non-small cell lung carcinomas (NSCLCs); however, their protein expression status has not yet been fully elucidated. In this study we investigated ALK protein expression in 302 NSCLCs and 291 gastric carcinomas by means of immunohistochemical analysis. Twelve (4.0%) NSCLCs, but none of the gastric carcinomas, were found to be positive for ALK. The ALK signal was detected in the cytoplasm of cancer cells. Subsequent RNA analysis of 10 RNA-available, immunohistochemically ALK-positive tumors revealed that three tumors had EML4-ALK variant 1, three tumors had variant 2, three tumors had variants 3a and 3b, and one tumor had a novel variant in which exon 14 of EML4 is connected to the nucleotide at position 53 of exon 20 of ALK by a 2-bp insertion. These results suggest that immunohistochemical ALK detection is a useful way to screen NSCLCs for tumors containing ALK fusions.

Introduction

Structural chromosome aberrations that result in the production of fusion oncogenes are one of the most common causes of oncogenesis. In the past they have been reported in many classes of hematological malignancies and mesenchymal tumors (1,2), and recently in a few types of epithelial carcinomas (3-5). A fusion gene comprising portions of the *EML4* gene and the *ALK* gene that resulted from a small inversion in chromosome 2p was recently discovered in a subset of non-small cell lung carcinomas (NSCLCs) (4). The fused mRNA based on the gene fusion encodes the N-terminal portion of EML4 ligated to the intracellular region of the receptor-type protein tyrosine kinase ALK. EML4-ALK oligomerizes constitutively in cells through the coiled-coil domain within the EML4 region and becomes activated to exert oncogenicity both *in vitro* and *in vivo* (4,6). Several types of EML4-ALK variants have been found in NSCLCs (4,6-18), and although one NSCLC containing KIF5B-ALK and another NSCLC containing TFG-ALK have been found (13,15), all of the other ALK fusions detected in NSCLCs have been EML4-ALK fusions.

Notably, recent studies have shown that ALK inhibitors have potential therapeutic efficacy for NSCLCs that are positive for ALK fusion proteins (4,6,16,19). Thus, the development of a diagnostic system for NSCLCs expressing ALK fusion proteins will be essential to identifying subgroups of NSCLC patients for treatment with ALK inhibitors. Immunohistochemical analysis of paraffin-embedded sections during routine pathologic diagnosis is a convenient means of examining the level of protein expression when the analytical condition is determined. Takeuchi *et al* recently reported an effective means of immunohistochemical detection of EML4-ALK by the intercalated antibody-enhanced polymer (iAEP) method (13). However, another group reported difficulty detecting EML4-ALK immunohistochemically (14), and it is speculated that the low expression level of EML4-ALK protein may be attributable to a low level of EML4 transcriptional activity or to instability of EML4-ALK in cells (13). Moreover, based on the results of a fluorescence *in situ* hybridization (FISH) analysis, Perner *et al* reported finding that only a subset of tumor cells contains the 2p rearrangement that leads to the formation of EML4-ALK (10). Thus, a system for immunohistochemical detection of ALK in NSCLCs would need to be established in order to diagnose tumors containing ALK fusions and elucidate the expression status of ALK fusion proteins. We also believe that immunohistochemical screening for ALK fusions may lead to the identification of novel EML4-ALK variants or novel fusions with ALK in addition to known EML4-ALK variants. Moreover, although the only carcinomas in

Correspondence to: Dr Kazuya Shinmura, First Department of Pathology, Hamamatsu University School of Medicine, 1-20-1 Handayama, Higashi Ward, Hamamatsu 431-3192, Japan
E-mail: kzshinmu@hama-med.ac.jp

Key words: EML4, ALK, non-small cell lung carcinoma, fusion transcript, immunohistochemistry

which ALK fusions have been found thus far are NSCLCs, ALK fusions may be present in other types of carcinomas. However, no studies using the iAEP method, except a study by Takeuchi *et al* (13), have been published. Therefore, in the present study, we immunohistochemically evaluated a total of 302 NSCLCs and 291 gastric carcinomas for ALK expression using the iAEP method and then investigated RNA-available, immunohistochemically ALK-positive tumors for expression of EML4-, KIF5B- and TFG-ALK fusions.

Materials and methods

Surgical specimens. Samples of surgical specimens from 302 NSCLC and 291 gastric carcinoma patients who underwent surgery for their cancer at Hamamatsu University School of Medicine, University Hospital or Mikatahara Seirei General Hospital were obtained. The mean age of the 302 NSCLC patients was 63.9 years [standard deviation (SD) 10.7], and they consisted of 168 men and 134 women. The NSCLC tumors were histologically classified as adenocarcinoma in 184 cases, squamous cell carcinoma in 98 cases, large-cell carcinoma in 9 cases and adenosquamous carcinoma in 11 cases. The mean age of the 291 gastric carcinoma patients was 65.4 years (SD 11.8), and they consisted of 206 men and 85 women. The gastric tumors were histologically classified as intestinal-type adenocarcinoma in 151 cases, diffuse-type adenocarcinoma in 138 cases and adenosquamous carcinoma in 2 cases. This study was approved by the Institutional Review Board (IRB) of Hamamatsu University School of Medicine and the IRB of Mikatahara Seirei General Hospital.

Immunohistochemical staining. Immunostaining for ALK using the iAEP method was performed as described previously (13) with slight modifications. In brief, paraffin-embedded tissue sections were deparaffinized, rehydrated and boiled at 96˚C for 40 min in Target Retrieval Solution (pH 9.0) (Dako, Kyoto, Japan) for antigen retrieval. Endogenous peroxidase activity was blocked by incubation for 5 min in a 3% hydrogen peroxide solution. Next, the sections were incubated with a Protein Block, Serum-free (Dako) for 10 min at room temperature (RT) and then with a mouse anti-ALK monoclonal antibody (clone 5A4; Abcam, Cambridge, UK) at a dilution of 1:50 for 30 min at RT. To increase the sensitivity of detection, the sections were incubated with polyclonal rabbit anti-mouse immunoglobulin at a dilution of 1:500 for 15 min at RT. After washing, the sections were incubated for 30 min at RT with an amino acid polymer conjugated with goat anti-rabbit IgG and horseradish peroxidase (Histofine Simple Stain MAX-PO Kit; Nichirei, Tokyo, Japan). The antigen-antibody complex was visualized with 3,3'-diaminobenzidine tetrahydrochloride, and the sections were counterstained with hematoxylin. The staining was performed with a Dako autostainer (Dako) (20).

Reverse transcription (RT)-polymerase chain reaction (PCR). Total RNA was extracted from lung tissue samples with an RNeasy Kit (Qiagen, Valencia, CA, USA) and converted to first-strand cDNA with a SuperScript First-Strand Synthesis System for RT-PCR (Invitrogen, Carlsbad, CA, USA) by following the supplier's protocol. PCR was performed in 20-μl reaction mixtures containing HotStarTaq DNA polymerase (Qiagen) under the following conditions: 30 sec at 94˚C, 30 sec at 61˚C and 90 sec at 72˚C for 45 cycles. A total of five different PCR primer pairs for EML4-ALK, three PCR primer pairs for KIF5B-ALK and one PCR primer pair for TFG-ALK were used for the RT-PCR. The forward PCR primers were: 5'-GCC TCA GTG AAA AAA TCA GTC TCA AG-3' for the sequence on exon 2 of EML4, 5'-ACA AAT TCG AGC ATC ACC TTC TCC-3' for the sequence on exon 4 of EML4, 5'-GTG CAG TGT TTA GCA TTC TTG GGG-3' for the sequence on exon 13 of EML4, 5'-CTG TGG GAT CAT GAT CTG AAT CCT G-3' for the sequence on exon 14 of EML4, 5'-CTT CCT GGC TGT AGG ATC TCA TGA C-3' for the sequence on exon 19 of EML4, 5'-CAC TAT TGT AAT TTG CTG CTC TCC ATC ATC-3' for the sequence on exon 10 of KIF5B, 5'-AAT CTG TCG ATG CCC TCA GTG AAG-3' for the sequence on exon 17 of KIF5B, 5'-TGA TCG CAA ACG CTA TCA GCA AG-3' for the sequence on exon 24 of KIF5B and 5'-TCG TTT ATT GGA TAG CTT GGA ACC AC-3' for the sequence on exon 4 of TFG. The reverse PCR primer used was the same, i.e., 5'-GAG GTC TTG CCA GCA AAG CAG TAG-3' for the sequence on exon 20 of ALK. The PCR products were fractionated by electrophoresis on an agarose gel and stained with ethidium bromide. The PCR-amplified products were purified with a PCR purification kit (Qiagen) and directly sequenced with a BigDye Terminator Cycle Sequencing Reaction Kit (Applied Biosystems, Tokyo, Japan) and the ABI 3100 Genetic Analyzer (Applied Biosystems) as described previously (7). The reference sequences for the *ALK*, *EML4*, *KIF5B* and *TFG* genes are accession numbers NM_004304, NM_019063, NM_004521 and NM_006070, respectively.

Statistical analysis. Statistical comparisons were performed by the two-tailed Student's t-test with Excel software (Microsoft Corp., Redmond, WA, USA).

Results

Immunohistochemical detection of ALK-positive NSCLCs. Samples of 302 NSCLCs and 291 gastric carcinomas were immunohistochemically stained for ALK with 5A4 anti-ALK monoclonal antibody using the iAEP method, and 12 (4.0%) of the NSCLCs and none (0%) of the gastric carcinomas were positive for ALK expression (Table I). ALK staining was observed in the cytoplasm of the cancer cells in all 12 NSCLCs, but not in any of the non-cancerous cells (Fig. 1). The mean age of the NSCLC patients whose tumors were positive for ALK was 57.3 years (SD 15.7) and significantly lower than the mean age of the NSCLC patients whose tumors were negative for ALK (64.2 years of age, SD 10.4) (p=0.027). The NSCLC patients whose tumors were positive for ALK consisted of 6 men and 6 women, and the ALK-positive NSCLC tumors were classified histologically as adenocarcinoma in 10 cases, adenosquamous carcinoma in 1 case and squamous cell carcinoma in 1 case (Table I).

Detection of various EML4-ALK fusion transcripts in NSCLCs. Next, 10 RNA-available, ALK-positive NSCLCs were investigated for expression of EML4-, KIF5B- and TFG-ALK fusion transcripts by RT-PCR and subsequent sequencing

Table I. Clinicopathological information and EML4-ALK fusions detected in immunohistochemically ALK-positive NSCLCs.

No.	Age	Gender	Histopathological diagnosis	EML4-ALK transcript
1	48	Female	Adenocarcinoma	Variant 1
2	49	Male	Adenocarcinoma	Variant 1
3	66	Male	Adenocarcinoma	Variant 1
4	46	Female	Adenocarcinoma	Variant 2
5	57	Male	Adenocarcinoma	Variant 2
6	79	Male	Adenocarcinoma	Variant 2
7	33	Female	Adenosquamous carcinoma	Variants 3a and 3b
8	63	Female	Adenocarcinoma	Variants 3a and 3b
9	83	Male	Adenocarcinoma	Variants 3a and 3b
10	58	Male	Adenocarcinoma	A novel variant[a]
11	36	Female	Adenocarcinoma	Not examined[b]
12	69	Female	Squamous cell carcinoma	Not examined[b]

[a]Exon 14 of EML4 is connected to a 2-bp fragment that in turn is ligated to the nucleotide at position 53 of exon 20 of ALK. [b]Due to the absence of an RNA sample, RT-PCR analysis for ALK fusions was not performed.

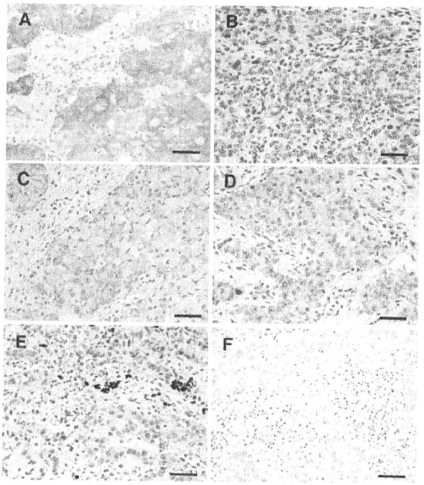

Figure 1. Representative results of immunohistochemical staining for ALK in non-small cell lung carcinomas. ALK protein expression was detected with 5A4 anti-ALK monoclonal antibody by the intercalated antibody-enhanced polymer method. A, B, C, D and E are the adenocarcinomas in cases No. 2, 5, 6, 8 and 10, respectively. F is the adenocarcinoma which showed no ALK expression. Bar, 50 μm.

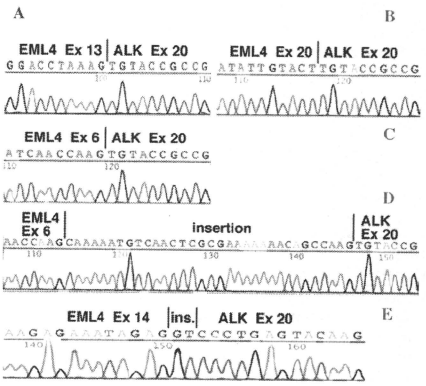

Figure 2. Detection of EML4-ALK fusion transcripts in non-small cell lung carcinomas. (A) EML4-ALK variant 1 transcript detected in case No. 1. (B) EML4-ALK variant 2 transcript detected in case No. 4. (C and D) EML4-ALK variants 3a (C) and 3b (D) transcripts detected in case No. 7. (E) Novel EML4-ALK transcript variant detected in case No. 10.

analyses. As a negative control, we also performed an RT-PCR analysis of 30 randomly selected, immunohistochemically ALK-negative NSCLCs. No expression of KIF5B-ALK or TFG-ALK fusion transcripts was detected in any of the carcinomas, but EML4-ALK fusion transcripts were detected in all 10 RNA-available, ALK-positive NSCLCs (Table I). As expected, no RT-PCR products were detected in any of the 30 immunohistochemically ALK-negative NSCLCs. Regarding the type of the EML4-ALK transcript, in 3 cases (No. 1-3) the fusion was variant 1, a fusion between exon 13 of EML4 and exon 20 of ALK (Fig. 2A), and in 3 cases (No. 4-6) it was variant 2, a fusion between exon 20 of EML4 and exon 20 of ALK (Fig. 2B). In 3 other cases (No. 7-9) the RT-PCR analysis yielded two bands, and they corresponded to variant 3a, a fusion between exon 6 of EML4 and exon 20 of ALK (Fig. 2C), and variant 3b, a fusion containing an additional 33-bp sequence derived from intron 6 of EML4 between exon 6 of EML4 and exon 20 of ALK (Fig. 2D). Notably, in case No. 10,

sequencing of the RT-PCR product revealed that exon 14 of EML4 was connected to an unidentified 2-bp fragment that was in turn ligated to the nucleotide at position 53 of exon 20 of ALK (Fig. 2E). The EML4-ALK sequence detected in case No. 10 allows an in-frame connection between the two genes and is a novel variant. The mean age of the 10 NSCLC patients whose tumors contained EML4-ALK transcripts was 58.2 years (SD 15.3), and they consisted of 6 men and 4 women. The NSCLC tumors containing EML4-ALK transcripts were histologically classified as adenocarcinoma in 9 cases and adenosquamous carcinoma in 1 case. These findings suggest that the iAEP method is useful for screening paraffin-embedded tissue sections for NSCLCs containing ALK fusion transcripts.

Discussion

Immunohistochemical screening for ALK expression using the iAEP method in the present study revealed an immunohistochemical ALK signal in 12 (4.0%) of 302 NSCLCs but not in any of the 291 gastric carcinomas. The ALK signal was detected in the cytoplasm of the cancer cells in all of the ALK-positive NSCLCs. RT-PCR and subsequent sequencing analyses of RNA from the 10 RNA-available, ALK-positive NSCLCs revealed the EML4-ALK variant 1 in 3 cases, variant 2 in 3 cases, both variants 3a and 3b in 3 cases, and a novel variant consisting of a fusion between exon 14 of EML4 and a nucleotide within exon 20 of ALK in 1 case. These results suggest that the immunohistochemistry-based system is useful for screening NSCLCs for ALK fusions, and identification of a novel EML4-ALK variant would be helpful in diagnosing NSCLCs containing ALK fusions in the future.

The proportion of immunohistochemically ALK-positive NSCLCs in this study (4.0%) is almost the same as the proportions of NSCLCs containing ALK fusion transcripts reported in previous studies (4,6-18), and in the present study EML4-ALK variants were detected in all RNA-available, immunohistochemically ALK-positive NSCLCs. These results suggest that our immunohistochemical analysis was performed properly and that the iAEP method with 5A4 anti-ALK antibody is a useful diagnostic tool for screening for NSCLCs containing ALK fusion proteins.

The histopathological diagnosis of 10 of the 12 immunohistochemically ALK-positive NSCLCs and 9 of the 10 EML4-ALK-positive NSCLCs in this study was adenocarcinoma. The predominance of adenocarcinomas among EML4-ALK-positive NSCLCs is consistent with the results of previous studies (6,12). This finding is also consistent with the recent finding of the growth of hundreds of adenocarcinoma nodules in transgenic mice in which EML4-ALK mRNA was transcribed specifically in lung epithelial cells (21). In the present study the mean age of the patients with immunohistochemically ALK-positive NSCLCs was significantly lower than that of the patients with ALK-negative NSCLCs. Although the mechanism responsible for the age difference is unknown, early onset may be a characteristic of ALK fusion-positive NSCLCs.

A novel EML4-ALK variant was found in this study. In this novel variant, exon 14 of EML4 was connected to a 2-bp fragment that was in turn ligated to the nucleotide at position 53 of exon 20 of ALK. Notably, the connection in each of two EML4-ALK variants, 4 and 7, is known to be between exon 14 of EML4 and a nucleotide within exon 20 of ALK (11,13). In variant 4, exon 14 of EML4 is connected to an unidentified 11-bp cDNA fragment that in turn is ligated to the nucleotide at position 50 of exon 20 of ALK (11), while in variant 7, exon 14 of EML4 is connected to the nucleotide at position 13 of exon 20 of ALK (13). Thus, the variant identified in this study is the third variant with a connection between exon 14 of EML4 and a nucleotide within exon 20 of ALK. Connections located within, rather that at the 5' terminus of, exon 20 of ALK have also been reported in MSN-ALK and MYH9-ALK, both of which have been detected in anaplastic large-cell lymphoma (22,23). Since a systemic understanding of the ALK fusions is important to correctly diagnose NSCLCs containing ALK fusions, our identification of a novel EML4-ALK variant should contribute to establishing a practical and accurate diagnostic system in the future.

Since the intracellular region of ALK was used as the antigen to produce the 5A4 anti-ALK antibody used in this study, both EML4-ALK and wild-type ALK should have been detected by the antibody. Takeuchi *et al* attempted to determine whether both transcripts are expressed by quantitatively analyzing the amount of mRNA specific for wild-type ALK and ALK fusion transcript separately, and found that none of the EML4-ALK-positive tumors yielded a substantial amount of wild-type ALK mRNA (13). Thus, immunohistochemical staining with the 5A4 antibody using the iAEP method appears to detect ALK fusion proteins and not wild-type ALK in NSCLCs. Our results for detection of EML4-ALK variants in all of the RNA-available, immunohistochemically ALK-positive NSCLCs support this view.

Our immunohistochemical analysis did not detect ALK protein expression in any of the gastric carcinomas. This was the first search for ALK fusion proteins in gastric carcinomas, and the results clearly demonstrated the absence of ALK fusion in gastric carcinomas. Since previous RNA analyses showed no EML4-ALK transcripts in 96 gastric carcinomas (8) and 33 gastric carcinomas (11), our results are consistent. The only human carcinomas in which ALK fusions have ever been found are NSCLCs. However, since it is unknown whether ALK fusions are involved in the genesis and development of other types of carcinoma, it may be worth investigating various types of carcinomas for expression of ALK fusion proteins in the future.

Acknowledgements

We are grateful to Dr K. Takeuchi (Cancer Inst, JFCR) for his technical advice regarding the iAEP method. This study was supported, in part, by a Grant-in-Aid from the Ministry of Health, Labour and Welfare for the Comprehensive 10-Year Strategy for Cancer Control (19-19), by a Grant-in-Aid from the Japan Society for the Promotion of Science for Scientific Research (no. 19790286), by a Grant-in-Aid from the Ministry of Education, Culture, Sports, Science and Technology of Japan on Priority Area (no. 18014009), by the 21st century COE program 'Medical Photonics' and by the Smoking Research Foundation.

References

1. Look AT: Oncogenic transcription factors in the human acute leukemias. Science 278: 1059-1064, 1997.
2. Lucansky V, Sobotkova E, Tachezy R, Duskova M and Vonka V: DNA vaccination against ber-abl-positive cells in mice. Int J Oncol 35: 941-951, 2009.
3. Tomlins SA, Rhodes DR, Perner S, Dhanasekaran SM, Mehra R, Sun XW, Varambally S, Cao X, Tchinda J, Kuefer R, Lee C, Montie JE, Shah RB, Pienta KJ, Rubin MA and Chinnaiyan AM: Recurrent fusion of TMPRSS2 and ETS transcription factor genes in prostate cancer. Science 310: 644-648, 2005.
4. Soda M, Choi YL, Enomoto M, Takada S, Yamashita Y, Ishikawa S, Fujiwara S, Watanabe H, Kurashina K, Hatanaka H, Bando M, Ohno S, Ishikawa Y, Aburatani H, Niki T, Sohara Y, Sugiyama Y and Mano H: Identification of the transforming EML4-ALK fusion gene in non-small cell lung cancer. Nature 448: 561-566, 2007.
5. Verdorfer I, Fehr A, Bullerdiek J, Scholz N, Brunner A, Krugmann J, Hager M, Haufe H, Mikuz G and Scholtz A: Chromosomal imbalances, 11q21 rearrangement and MECT1-MAML2 fusion transcript in mucoepidermoid carcinomas of the salivary gland. Oncol Rep 22: 305-311, 2009.
6. Mano H: Non-solid oncogenes in solid tumors: EML4-ALK fusion genes in lung cancer. Cancer Sci 99: 2349-2355, 2008.
7. Shinmura K, Kageyama S, Tao H, Bunai T, Suzuki M, Kamo T, Takamochi K, Suzuki K, Tanahashi M, Niwa H, Ogawa H and Sugimura H: EML4-ALK fusion transcripts, but no NPM-, TPM3-, CLTC-, ATIC-, or TFG-ALK fusion transcripts, in non-small cell lung carcinomas. Lung Cancer 61: 163-169, 2008.
8. Fukuyoshi Y, Inoue H, Kita Y, Utsunomiya T, Ishida T and Mori M: EML4-ALK fusion transcript is not found in gastrointestinal and breast cancers. Br J Cancer 98: 1536-1539, 2008.
9. Choi YL, Takeuchi K, Soda M, Inamura K, Togashi Y, Hatano S, Enomoto M, Hamada T, Haruta H, Watanabe H, Kurashina K, Hatanaka H, Ueno T, Takada S, Yamashita Y, Sugiyama Y, Ishikawa Y and Mano H: Identification of novel isoforms of the EML4-ALK transforming gene in non-small cell lung cancer. Cancer Res 68: 4971-4976, 2008.
10. Perner S, Wagner PL, Demichelis F, Mehra R, Lafargue CJ, Moss BJ, Arbogast S, Soltermann A, Weder W, Giordano TJ, Beer DG, Rickman DS, Chinnaiyan AM, Moch H and Rubin MA: EML4-ALK fusion lung cancer: a rare acquired event. Neoplasia 10: 298-302, 2008.
11. Takeuchi K, Choi YL, Soda M, Inamura K, Togashi Y, Hatano S, Enomoto M, Takada S, Yamashita Y, Satoh Y, Okumura S, Nakagawa K, Ishikawa Y and Mano H: Multiplex reverse transcription-PCR screening for EML4-ALK fusion transcripts. Clin Cancer Res 14: 6618-6624, 2008.
12. Inamura K, Takeuchi K, Togashi Y, Hatano S, Ninomiya H, Motoi N, Mun MY, Sakao Y, Okumura S, Nakagawa K, Soda M, Choi YL, Mano H and Ishikawa Y: EML4-ALK lung cancers are characterized by rare other mutations, a TTF-1 cell lineage, an acinar histology and young onset. Mod Pathol 22: 508-515, 2009.
13. Takeuchi K, Choi YL, Togashi Y, Soda M, Hatano S, Inamura K, Takada S, Ueno T, Yamashita Y, Satoh Y, Okumura S, Nakagawa K, Ishikawa Y and Mano H: KIF5B-ALK, a novel fusion oncokinase identified by an immunohistochemistry-based diagnostic system for ALK-positive lung cancer. Clin Cancer Res 15: 3143-3149, 2009.
14. Martelli MP, Sozzi G, Hernandez L, Pettirossi V, Navarro A, Conte D, Gasparini P, Perrone F, Modena P, Pastorino U, Carbone A, Fabbri A, Sidoni A, Nakamura S, Gambacorta M, Fernández PL, Ramirez J, Chan JK, Grigioni WF, Campo E, Pileri SA and Falini B: EML4-ALK rearrangement in non-small cell lung cancer and non-tumor lung tissues. Am J Pathol 174: 661-670, 2009.
15. Rikova K, Guo A, Zeng Q, Possemato A, Yu J, Haack H, Nardone J, Lee K, Reeves C, Li Y, Hu Y, Tan Z, Stokes M, Sullivan L, Mitchell J, Wetzel R, Macneill J, Ren JM, Yuan J, Bakalarski CE, Villen J, Kornhauser JM, Smith B, Li D, Zhou X, Gygi SP, Gu TL, Polakiewicz RD, Rush J and Comb MJ: Global survey of phosphotyrosine signaling identifies oncogenic kinases in lung cancer. Cell 131: 1190-1203, 2007.
16. Koivunen JP, Mermel C, Zejnullahu K, Murphy C, Lifshits E, Holmes AJ, Choi HG, Kim J, Chiang D, Thomas R, Lee J, Richards WG, Sugarbaker DJ, Ducko C, Lindeman N, Marcoux JP, Engelman JA, Gray NS, Lee C, Meyerson M and Jänne PA: EML4-ALK fusion gene and efficacy of an ALK kinase inhibitor in lung cancer. Clin Cancer Res 14: 4275-4283, 2008.
17. Horn L and Pao W: EML4-ALK: honing in on a new target in non-small cell lung cancer. J Clin Oncol 27: 4232-4235, 2009.
18. Shaw AT, Yeap BY, Mino-Kenudson M, Digumarthy SR, Costa DB, Heist RS, Solomon B, Stubbs H, Admane S, McDermott U, Settleman J, Kobayashi S, Mark EJ, Rodig SJ, Chirieac LR, Kwak EL, Lynch TJ and Iafrate AJ: Clinical features and outcome of patients with non-small cell lung cancer who harbor EML4-ALK. J Clin Oncol 27: 4247-4253, 2009.
19. McDermott U, Iafrate AJ, Gray NS, Shioda T, Classon M, Maheswaran S, Zhou W, Choi HG, Smith SL, Dowell L, Ulkus LE, Kuhlmann G, Greninger P, Christensen JG, Haber DA and Settleman J: Genomic alterations of anaplastic lymphoma kinase may sensitize tumors to anaplastic lymphoma kinase inhibitors. Cancer Res 68: 3389-3395, 2008.
20. Shinmura K, Iwaizumi M, Igarashi H, Nagura K, Yamada H, Suzuki M, Fukasawa K and Sugimura H: Induction of centrosome amplification and chromosome instability in p53-deficient lung cancer cells exposed to benzo[a]pyrene diol epoxide (B[a]PDE). J Pathol 216: 365-374, 2008.
21. Soda M, Takada S, Takeuchi K, Choi YL, Enomoto M, Ueno T, Haruta H, Hamada T, Yamashita Y, Ishikawa Y, Sugiyama Y and Mano H: A mouse model for EML4-ALK-positive lung cancer. Proc Natl Acad Sci USA 105: 19893-19897, 2008.
22. Tort F, Pinyol M, Pulford K, Roncador G, Hernandez L, Nayach I, Kluin-Nelemans HC, Kluin P, Touriol C, Delsol G, Mason D and Campo E: Molecular characterization of a new ALK translocation involving moesin (MSN-ALK) in anaplastic large cell lymphoma. Lab Invest 81: 419-426, 2001.
23. Lamant L, Gascoyne RD, Duplantier MM, Armstrong F, Raghab A, Chhanabhai M, Rajcan-Separovic E, Raghab J, Delsol G and Espinos E: Non-muscle myosin heavy chain (MYH9): a new partner fused to ALK in anaplastic large cell lymphoma. Genes Chromosomes Cancer 37: 427-432, 2003.

Cancer Science
The official journal of the Japanese Cancer Association JCA

Imaging mass spectrometry of gastric carcinoma in formalin-fixed paraffin-embedded tissue microarray

Yoshifumi Morita,[1,2] Koji Ikegami,[2] Naoko Goto-Inoue,[2] Takahiro Hayasaka,[2] Nobuhiro Zaima,[2] Hiroki Tanaka,[1] Takashi Uehara,[1] Tomohiko Setoguchi,[1] Takanori Sakaguchi,[1] Hisashi Igarashi,[3] Haruhiko Sugimura,[3] Mitsutoshi Setou[2,4] and Hiroyuki Konno[1]

[1]Second Department of Surgery, [2]Departments of Molecular Anatomy, and [3]Pathology, Hamamatsu University School of Medicine, Shizuoka, Japan

(Received June 6, 2009/Revised September 16, 2009/Accepted September 20, 2009/Online publication November 24, 2009)

The popularity of imaging mass spectrometry (IMS) of tissue samples, which enables the direct scanning of tissue sections within a short time-period, has been considerably increasing in cancer proteomics. Most pathological specimens stored in medical institutes are formalin-fixed; thus, they had been regarded to be unsuitable for proteomic analyses, including IMS, until recently. Here, we report an easy-to-use screening method that enables the analysis of multiple samples in one experiment without extractions and purifications of proteins. We scanned, with an IMS technique, a tissue microarray (TMA) of formalin-fixed paraffin-embedded (FFPE) specimens. We detected a large amount of signals from trypsin-treated FFPE-TMA samples of gastric carcinoma tissues of different histological types. Of the signals detected, 54 were classified as signals specific to cancer with statistically significant differences between adenocarcinomas and normal tissues. We detected a total of 14 of the 54 signals as histological type-specific with the support of statistical analyses. Tandem MS revealed that a signal specific to poorly differentiated cancer tissue corresponded to histone H4. Finally, we verified the IMS-based finding by immunohistochemical analysis of more than 300 specimens spotted on TMAs; the immunoreactivity of histone H4 was remarkably strong in poorly differentiated cancer tissues. Thus, the application of IMS to FFPE-TMA can enable high-throughput analysis in cancer proteomics to aid in the understanding of molecular mechanisms underlying carcinogenesis, invasiveness, metastasis, and prognosis. Further, results obtained from the IMS of FFPE-TMA can be readily confirmed by commonly used immunohistochemical analyses. (*Cancer Sci* 2010; 101: 267–273)

Intensive genome-based surveys are performed on candidate biomarker transcripts relevant to cancer tissues by utilizing the advances in high-throughput microarrays.[1,2] Further, various single-nucleotide polymorphism (SNP) analyses have been performed to further understand cancer.[3,4] Recently, cancer genome resequencing has been increasingly performed to acquire specific genomic data.[5,6] To achieve the systematic understandings of cancer by systems biology, data from genome resequencing and the corresponding data from the transcriptomes should be combined with the individual metabolome and proteome data of the cancer patient.[7]

Several approaches for the investigation of global alterations in proteomics have emerged. Mass spectrometry (MS) is used in combination with 2D electrophoresis or liquid chromatography.[8,9] Further, protein microarrays offer a means of effective identification of cancer-specific protein alterations to researchers.[10]

Despite the existence of techniques for the global detection of cancer-specific alterations at the protein level, proteomic approaches continue to possess two major disadvantages. Under most circumstances, proteomic approaches only allow a limited number of samples to be analyzed in an experiment. Additionally, proteomic techniques are not adopted for the investigation of large amounts of archival specimens that are stored in hospitals and medical institutes. TMAs have been developed for the analysis of a large number of specimens by antibody labeling.[11] It allows high-throughput profiling of the molecular and pathological alterations in tissue specimens.

In recent years, IMS has emerged and developed dramatically in the field of proteomics and metabolomics.[12,13] IMS enables simultaneous analysis of thousands of proteins directly from a tissue sample without protein extraction and usage of target-specific reagents such as antibodies.[14,15]

In this study, we combine the TMA and IMS technique, and introduce a simple and easy-to-use protocol to detect, by a single experimental trial, cancer-specific or histological type-specific proteins. Further, we optimized the IMS procedure for the FFPE samples that are commonly used in hospitals and stored for long time.

Materials and Methods

Specimens. We chose gastric cancer to perform the study for the evaluation of our experimental paradigm. Gastric cancer is the fourth most frequent cancer and the second leading cause of cancer-related death in the world.[16] In Japanese hospitals, large amounts of gastric cancer specimens are stored and are, thus, readily available to perform studies.

Human gastric cancer tissues and adjacent normal tissues were provided by the Diagnostic Pathology Division, Hospital of Hamamatsu University School of Medicine, Shizuoka, Japan. The study was performed in accordance with the guidelines for pathological specimen handling, which was approved by the ethical committee of the Hamamatsu University School of Medicine. Histological classification was based on Japanese Classification of Gastric Carcinoma, 2nd English edition.[17] Further, each tissue did not contain non-tumor tissue, confirmed by two pathologists.

For IMS, we used the old specimens which had been fixed in 10% neutral formalin promptly after surgery and had been stored for up to 2 years in paraffin. Tissue blocks of three cancer tissues and one adjacent normal tissue were cored using tissue microarrayer type KIN (Azumaya, Tokyo, Japan). A cylinder, 3 mm in diameter, was taken and placed into the recipient block. Three cancer tissues and one non-tumor gastric mucosal tissue were aligned as shown in Fig. 1a.

Sample preparation. For analysis, the FFPE tissue microarray blocks were sliced into 10-μm-thick serial sections; further, for hematoxylin–eosin staining, these blocks were sliced into 1-μm-thick sections, using a microtome (Tissue-Tek, Feather Trustome; Sakura Finetek, Tokyo, Japan). The analysis samples were deposited onto indium-tin-oxide (ITO)-coated glass slides

[4]To whom correspondence should be addressed.
E-mail: setou@hama-med.ac.jp

doi: 10.1111/j.1349-7006.2009.01384.x

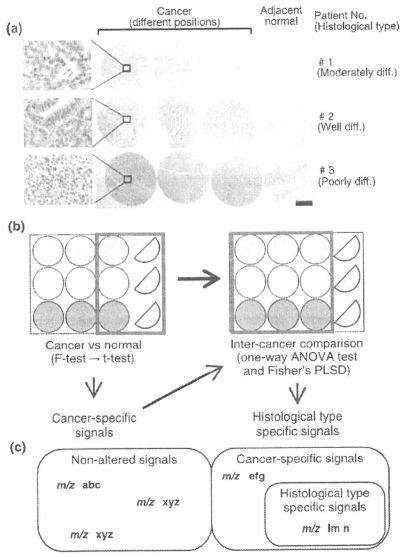

Fig. 1. Experimental paradigm design. (a) Formalin-fixed paraffin-embedded (FFPE) samples were cored with a 3-mm diameter needle and arranged in a line with three cancer tissues and one adjacent normal tissue. The histological type of the cancer of Patient 1 was moderately differentiated adenocarcinoma, that of Patient 2 was well-differentiated adenocarcinoma, and that of Patient 3 was poorly differentiated adenocarcinoma. Hematoxylin–eosin stain, ×10. Scale bar, 1 mm. Enclosed area corresponded to magnified microscopic image. Hematoxylin–eosin stain, ×400 (b) The schema of FFPE samples and the workflow of statistical analysis are shown. (c) The schema that categorizes the acquired signals is presented.

(Bruker Daltonics, Bremen, Germany), and the staining samples were loaded onto regular glass microscope slides by scooping the sections in a 50°C water bath, and then dried on an extender at 45°C. Paraffin was removed by 10-min immersion in xylene at 60°C. Subsequently, the slides were washed by stepwise immersions of 5-min duration each; this involved slide immersion in 100% ethanol twice, and once each in 90% ethanol, 80% ethanol, and 70% ethanol. After rehydration, these slides were incubated in a humid chamber at 55°C overnight.

Tryptic digestion. The sample slide was inserted into a slot on matrix-assisted laser desorption/ionization (MALDI) target plates affixed with conductive tape, and inserted into a chemical inkjet printer (CHIP-1000; Shimadzu, Kyoto, Japan). Trypsin solution was prepared by dissolving 20 μg of trypsin (Sigma, St. Louis, MO, USA) in 200 μL of 20-mM ammonium hydrogen carbonate (NH_4HCO_3). Trypsin microspotting was performed with CHIP-1000 in 5-nL droplets by five cycles of 1000 pl on each spot at a spatial interval of 250 μm. After spotting, MALDI target plates were incubated overnight at 37°C under high-humidity conditions.

Matrix deposition. The matrix solution was prepared by dissolving 50 mg of 2, 5-dihydroxybenzooic acid (DHB: Bruker Daltonics) in 1 mL of 70% methanol/0.1% trifluoroacetic acid. DHB is a widely used matrix for lower molecules including peptides.[18] A thin matrix layer was applied to the surface of the plates using a 0.2-mm nozzle caliber airbrush (Procon Boy FWA Platinum; Mr. Hobby, Tokyo, Japan). The spraying distance was maintained at 15 cm from the tissue surface. The total amount of the matrix solution on each slide was 2–3 mL. The spraying technique enabled full matrix coverage over the entire tissue surface and facilitated co-crystallization of matrix and bio-molecules. A desalting process such as ethanol wash was not performed, since the process does not significantly improve DHB-assisted imaging mass spectrometry (IMS) and NH_4HCO_3 is a highly volatile buffer.[18,19]

Direct analysis of tissue sections by MALDI mass spectrometry. Mass spectra were acquired using the QSTAR XL (Applied Biosystems, Foster City, CA, USA), a hybrid quadrupole/time-of-flight mass spectrometer equipped with an orthogonal MALDI source and a pulsed YAG laser that was operated at a repetition rate of 100 Hz, and a power modulator. Spectra were acquired in positive ion mode. Spectra were acquired in the range of m/z 500–2000. Representative mass spectra were acquired using random laser irradiation-sections. The number of laser shots was 150. An alignment of the mass spectra was performed to compare the datasets using SpecAlign software (http://physchem.ox.ac.uk/~jwong/specalign/). The peak intensity value of the spectra was normalized by dividing them with the total ion current (TIC) as previously described.[20,21]

Imaging of tissue section by mass spectrometry. IMS was performed using orthogonal MALDI (oMALDI) server software by defining a region of interest around the tissue slice. The mechanical resolution, which is the value that refers to the length of the stepwise movement of the laser beam on the sample stage, was 300 μm × 300 μm, and the accumulation time per spot was about 2 s. The acquired mass spectra were visualized using BioMap software (http://www.maldi-msi.org). Molecular images were captured using this software by applying baseline correction to the spectra and integrating these spectra over the peak of interest. Alignment of these mass spectra was performed using SpecAlign software.

Tissue protein identification. The quadrupole ion trap time-of-flight mass spectrometer, namely, AXIMA-QIT (Shimadzu), was used to perform MS/MS analysis. In the MS/MS operation, the data acquisition conditions (i.e. the laser power, collision energy, and the number of laser irradiations) were adjusted to obtain good-quality mass spectra with high intensity and signal-to-noise ratios (S/N) in the fragmented peaks. MS/MS spectra were processed using the Mascot search engine (http://www.matrixscience.com) using the National Center for Biotechnology Information (NCBI)/basic local alignment search tool (BLAST) protein database (http://blast.ncbi.nlm.nih.gov/Blast.cgi) with a taxonomy filter for humans, and the peptide and MS/MS tolerance at 0.3 Da. The search criteria was allowed to consider up to one missed cleavage and variable modifications including protein N-terminus acetylation, histidine/tryptophan oxidation, and methionine oxidation.

Statistical analysis. All statistical analyses were performed with StatView software version 5.0 (SAS Institute, Cary, NC, USA). First, statistical analyses were performed on adjoining cancer and normal tissue. The Student's t-test ($\alpha = 0.05$) was performed between peak intensity means of cancer and normal tissue samples on the basis of equal variance. Welch's test for unequal variance ($\alpha = 0.05$) was performed between peak intensity means of cancer and normal tissues. The corresponding P-value, i.e. P (T t), was reported as a measure of significant statistical variability between conditions.

We extracted signals that showed significantly higher intensity in cancer than in normal tissue in the form of cancer-specific

doi: 10.1111/j.1349-7006.2009.01384.x

peaks. To determine specific peaks related to the degree of differentiation, analysis of variance (ANOVA) and Fisher's protected least significant difference (PLSD) were performed as post-hoc tests on three histological types of three different cancer tissue samples. Fig. 1b shows the statistical workflow.

Immunohistochemical staining for histone H4. For immunohistochemistry (IHC), we used the formalin-fixed tissue microarray specimens containing a wide range of preservation time, up to 30 years after being embedded in paraffin. Each TMA was composed of 50 primary gastric tumors such as adenocarcinoma of various grades of differentiation. Three micrometer sections were cut from the TMA blocks. Immunostaining was performed by the Dako Autostainer System (Dako Japan, Tokyo, Japan) according to the manufacturer-recommended procedure. In brief, paraffin was removed by immersing the TMA slides in xylene for 5 min twice. Subsequently, the tissue sections were rehydrated by immersing the slides in 100% ethanol for 10 min twice, followed by two-time 10-min immersion in 95% ethanol. After rehydration, these slides were incubated at 96°C for 40 min in 10 mM sodium citrate buffer pH 6.0 and then cooled on the bench top for 20 min. Then, these sections were incubated in 3% hydrogen peroxide for 5 min and washed in Tris-buffered saline. A monoclonal antibody against histone H4 (L64C1; Cell Signaling Technology, Danvers, MA, USA) was used as the primary antibody at a dilution of 1:300. N-Histofine® Simple Stain MAX-PO (Multi) (Nichirei Biosciences, Tokyo, Japan) was used as the secondary antibody. After removing the secondary antibody, the sections were exposed to diaminobenzidine for 5 min, and then washed with distilled water. Counterstaining was performed with hematoxylin for 10 s.

IHC evaluation. The IHC evaluation was carried out in two independent ways by two of the authors (Y.M. and H.S.). An evaluation was performed by visual inspection, where IHC staining was classified into four ranks (0, negative; 1, slightly positive; 2, positive; 3, strongly positive) for common types of gastric carcinoma. Papillary adenocarcinoma was interpreted as well-differentiated adenocarcinoma and signet-ring cell carcinoma as poorly differentiated adenocarcinoma. Assignment of mucinous carcinoma category was made according to the other predominant elements. Special types of gastric carcinoma and other tumors were excluded. In total, 169 specimens were evaluated; they included 42 well-differentiated, 38 moderately differentiated, and 89 poorly differentiated adenocarcinomas. As described,[22] Steel–Dwass' test was performed by using free software available on a web site, MEPHAS (http://www.gen-info.osaka-u.ac.jp/testdocs/tomocom/). Another evaluation was carried out by quantifying the signal intensity of IHC staining with Scion image software version 4.0.3.2 (Scion, Frederick, MD, USA). We analyzed additional 170 specimens containing 43 well-differentiated, 40 moderately differentiated, and 87 poorly differentiated adenocarcinomas. The data were represented as the mean value of intensity ± SD. ANOVA and Fisher's PSLD were performed as post-hoc test among three histological types (well, moderately, and poorly differentiated).

Results

Experimental paradigm design. To statistically detect cancer-specific signals, we placed three cancer tissues and one normal tissue from three patients in a TMA. The histological type of cancer differed among the three patients (Fig. 1a). The sample from Patient 1 was moderately differentiated adenocarcinoma, that from Patient 2 was well-differentiated adenocarcinoma, and that from Patient 3 was poorly differentiated adenocarcinoma. We acquired tissue samples from three different regions of each patient for further statistical analysis to detect signals specific to cancer-differentiation status (Fig. 1a). During the first screening, we compared signals of three individual cancers with those of normal tissues (Fig. 1b). Thereafter, we screened the detected cancer-specific peaks by multiple comparisons of three different cancer regions belonging to three histological types (Fig. 1b). We categorize the obtained results on the basis of the statistical workflow in Fig. 1c.

Acquisition of mass spectra from FFPE-TMA samples. A previous report showed relatively weak signal intensities and low S/N ratio was obtained with FFPE tissue samples compared to freshly frozen ones.[23] We first examined if peptide signals could be sufficiently detected with FFPE-TMA. We employed chemical inkjet technology to equalize the quantity and the interval of trypsin solution application.[14] We detected vast quantities of signals that were sufficient to generate imaging data from FFPE-TMA samples. Figure 2 shows representative spectra obtained from three individual cancer tissues and normal tissues. The peaks obtained were mainly concentrated below m/z 2000 and could hardly be detected over m/z 2000. Thus, using SpecAlign, we performed signal-intensity normalization.

Detection of cancer specifically increased signals in IMS of digested FFPE tissue microarray. Subsequently, we performed IMS of FFPE-TMA on the samples and obtained mass spectra. We setup a spatial interval of 300 μm to prevent repeated laser irradiation, as the irradiated laser diameter was 200 μm. We completed the scanning of the TMA samples with 12 spots in approximately 1 h. We detected a total of 72 signals with FFPE-TMA samples. Fig. S1 shows the obtained array images. To perform statistical data analysis, we quantified the signal intensities of m/z peaks. The first statistical screening (Fig. 1b) revealed 54 signals, the intensity of which was detected to be significantly increased in cancer tissues (Fig. 3). We examined the reliability of this screening by performing two independent trials with sibling arrays. Forty of the 54 signals were detected in the two independent trials (Fig. 3). Figure 4(a) shows the representative array result of the signal significantly increased in cancer. In contrast, Fig. 4b shows that another signal has no significant difference between cancer and normal tissues, i.e. it shows an even distribution pattern.

Detection of histological type-specific increased signals in IMS of digested FFPE tissue microarray. We further analyzed the quantified signal intensities to examine whether such histological type-specific signals could be detected with our experimental paradigm. To this end, we compared signals detected in cancer tissues among the well-differentiated, moderately differentiated, and poorly differentiated tissues (Fig. 1b). To detect specific signals, we conducted statistical analyses with one-way ANOVA followed by Fisher's PLSD. Certain signals demonstrating a cancer-specific pattern appeared to demonstrate uneven signal intensities in different degrees of cancer differentiation (Fig. 3, Fig. 5a–c). Of the detected signals, peaks having m/z 537.2, 1168.4, 1387.6, 1475.8 were reproducibly detected in another experimental trial. Other signals were detected only once in two experimental trials. Owing to the two-step screening, it is probable that the detection of histological type-specific signals shows worse reproducibility than the simple detection of cancer-specific signals.

Identification of protein-specific increase in poorly differentiated cancer tissues by MS/MS analysis. We attempted to identify the signals that were specifically detected in poorly differentiated cancer tissue. We performed MS/MS analyses on the FFPE-TMA, and analyzed the resultant data with the Mascot search engine. We identified one signal with an m/z 1325.6 as histone H4 that is specific to poorly differentiated cancers (Fig. 6a), and identified a protein that demonstrated non-specific expression and had an m/z 976.4 corresponding to that of actin (Fig. 6b). Other peaks could not be detected due to their weak intensity.

IHC staining for histone H4 using another TMA specimen of larger numbers of the cases. Finally, we examined whether

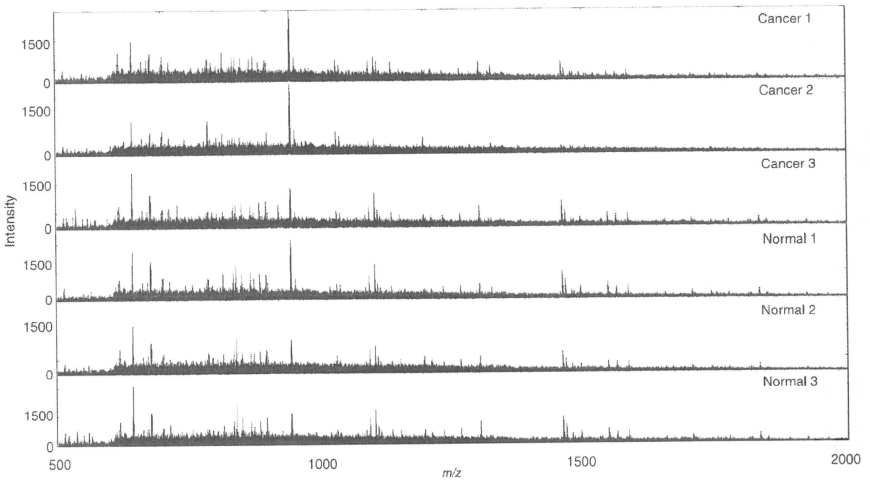

Fig. 2. Acquired mass spectra from formalin-fixed paraffin-embedded (FFPE) tissue microarray samples (TMA) by random laser irradiation. Acquired mass spectra from each TMA spot of adjoining cancer and normal tissue are shown as representative spectra. *m/z* refers to mass per charge ratio.

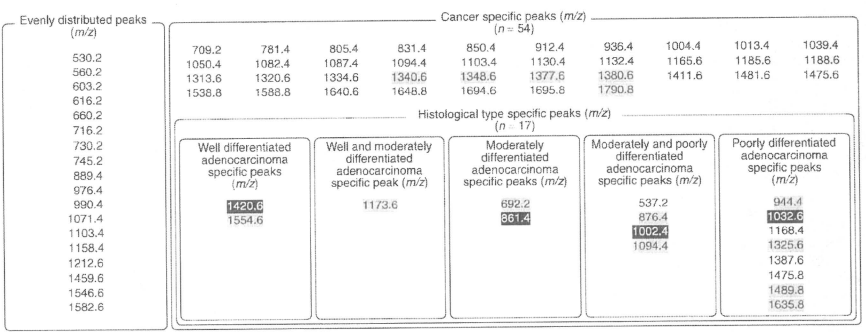

Fig. 3. The peak list acquired from mass spectra. The shaded values represent signals that showed significantly increased intensity in cancer tissues in one independent trial ($P < 0.05$). The white-on-black values represent signals that showed significant difference among three cancers in one independent trial ($P < 0.05$).

histone H4 was specifically strongly detected in poorly differentiated cancers. In total, we stained 400 gastric tumors including adenocarcinoma, squamous carcinoma, neuroendocrine carcinoma, metastatic carcinoma, malignant lymphoma, and adenoma. We excluded 61 specimens such as a special type of gastric carcinoma, malignant lymphoma, and benign lesion. We examined 339 gastric carcinomas composed of 85 well-differentiated carcinomas, 78 moderately differentiated carcinomas, and 176 poorly differentiated carcinomas. Figure 7(a) shows representative photomicrographs of each histological type. We evaluated the result of IHC in two approaches. First, we determined the staining appearance according to four ranks (0, negative; 1, slightly positive; 2, positive; 3, strongly positive). Slightly positive and positive staining reached a high rate in well- and moderately differentiated carcinoma. In contrast, poorly differentiated adenocarcinomas were categorized into much more positive staining such as rank 2 or rank 3 (Fig. 7b). Second, we also performed more quantitative analysis. We

doi: 10.1111/j.1349-7006.2009.01384.x

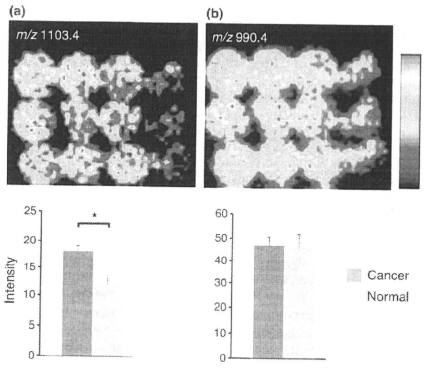

Fig. 4. Cancer-specific signal increase and even distribution of signals in imaging mass spectrometry (IMS) of digested formalin-fixed paraffin-embedded (FFPE) tissue microarrays (TMA). (a) Significantly strong peak intensity was detected at m/z 1103.4. (b) No significant difference was observed between cancer and normal tissues at an m/z of 990.4. Values are represented as mean ± SD (n = 3). $^*P < 0.05$.

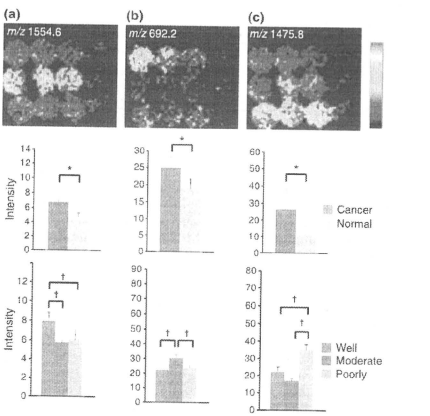

Fig. 5. Histological type-specific signal increase in imaging mass spectrometry (IMS) of digested formalin-fixed paraffin-embedded (FFPE) tissue microarrays (TMA). (a) Ion imaging revealed a peak with significantly strong signal intensity in well-differentiated adenocarcinoma at an m/z of 1554.6. (b) Ion imaging revealed a peak with significantly strong signal intensity in moderately differentiated adenocarcinoma at an m/z of 692.2. (c) Ion imaging revealed a peak with significantly strong signal intensity in poorly differentiated adenocarcinoma at m/z 1475.8. Values are represented as mean ± SD (n = 3). $^*P < 0.05$, $^\dagger P < 0.05$.

quantified the signal intensity using Scion image software. In agreement with our visual inspection, poorly differentiated carcinoma showed significantly higher value compared to well-differentiated or moderately differentiated carcinomas. There was no significant difference between well- and moderately differentiated carcinoma (Fig. 7c).

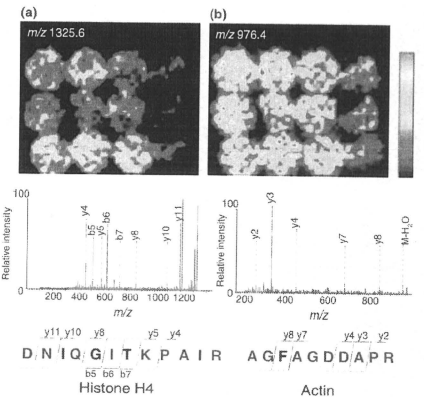

Fig. 6. MS/MS analysis of digested peptide and protein identification. (a) The biomolecule of an m/z 1325.6 was identified as histone H4. DNIQGITKPAIR: abbreviation of the amino-acid sequence aspartic acid–asparagine–isoleucine–glutamine–glycine–isoleucine–threonine–lysine–proline–alanine–isoleucine–arginine. y4, y5, y8, y10, y11 represent each fragment ion, which includes the C-terminal domain. b5, b6, b7 represent each fragment ion, which includes the N-terminal domain. (b) The biomolecule with an m/z 976.4 was identified as actin. AGFAGDDAPR: abbreviation for the amino-acid sequence alanine–glycine–phenylalanine–alanine–glycine–aspartic acid–aspartic acid–alanine–proline–arginine. y2, y3, y4, y7, y8 refer to each fragment ion, which includes the C-terminal domain.

Discussion

In this report, we presented a simple and easy-to-use method for the detection and identification of cancer-specific proteins, i.e. strong candidates for biomarkers or drug targets, with high reliability in an experimental trial (Fig. 1). We succeeded in detecting cancer-specific signals with 75% (40 per 54) reliability in two independent experiments (Fig. 3, Fig. 4). Furthermore, we detected signals that were specific for each status of cancer differentiation (Fig. 5). Finally, we successfully identified one of the signals that was specifically increased in the poorly differentiated cancer tissue as histone H4 (Fig. 6).

We analyzed 12 different tissue samples within 1 h. The TMA-IMS technique has prominent advantages when compared to existing proteomic techniques. This technique enables the analysis of multiple proteins in multiple tissue samples in just one experiment. The existing proteomic techniques lack either multiprocessing property with respect to the analysis of samples or detection of proteins. Proteomic techniques employing 2D electrophoresis-MS or protein microarrays can analyze only single or double samples in one experiment; however, they can detect and identify multiple proteins in one experiment. In contrast, the limitation of TMA is that it enables that analysis of only one or two proteins in one experiment; however, it enables simultaneous analysis of multiple tissue samples. Thus, the TMA-IMS technique has two advantages compared to existing techniques. Moreover, the TMA-IMS technique does not require

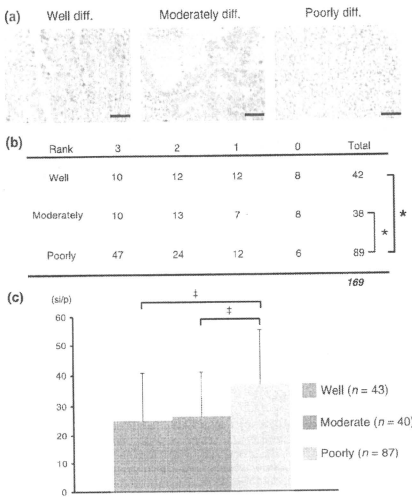

Fig. 7. Immunohistochemical (IHC) staining for histone H4. (a) Representative photomicrograph of IHC for histone H4 protein, ×400. Scale bar, 50 μm. (b) Evaluation of IHC according to four ranks (0, negative; 1, slightly positive; 2, positive; 3, strongly positive). The 169 gastric carcinomas comprised 42 well-differentiated carcinomas, 38 moderately differentiated carcinomas, 89 poorly differentiated carcinomas. *$P < 0.05$ by Steel–Dwass' test. (c) Quantitative analysis of IHC signal intensity. The 170 gastric carcinomas comprised 43 well-differentiated carcinomas, 40 moderately differentiated carcinomas, and 87 poorly differentiated carcinomas. Values are represented as mean ± SD. si/p, signal intensity per pixel. ‡$P < 0.01$.

the complicated sample-preparation steps which are required in 2-DE-MS-based proteomics.

The high-intensity signals detected from cancer tissues account for approximately two-thirds (54 of 72) of all signals detected. We failed to detect signals specific to normal tissues. This could be explained by the heterogeneity underlying normal tissues. The adjacent normal tissues consisted of varied types of tissues, such as mucosa, fatty tissue, and muscle. Acquired signal intensities in normal tissues were the average of whole spectrum derived from each of the tissues. Hence, tissue type-specific peaks were totally obscured, resulting in the failure to detect adjacent normal tissue-specific peaks.

We detected 17 histological type-specific peaks in two independent experiments. (Fig. 3) The reproducibility of signal detection from normal tissues was lower (4 per 17; 24%) than that of signal-detection from cancer tissues (75%). This could be explained by our experimental paradigm under which we performed two-step screening. The high severity of the first screening step excluded 9 of 13 peaks in either trial due to high variance among cancer tissues. In this technique, the two-step screening is essential as we cannot rule out the possibility of detecting false positive signals that are specific merely for certain patients. This problem could be addressed by spotting more samples under a variety of cancer tissue conditions in a TMA and performing multiple direct comparisons.

We identified from IMS screening histone H4 as a protein that is specifically increased in poorly differentiated adenocarcinoma (Fig. 6a). To validate the IMS result, we performed IHC for histone H4 protein using large amount of archival TMA specimens composed of various cellular density. In both visual inspection and quantitative analysis of IHC, histone H4 was strongly detected in poorly differentiated carcinoma (Fig. 7b,c). Similar strong detection of histone H4 in a cancer tissue has been reported by a recent study on a mouse model of brain tumor analyzed by IMS.[24] Dynamic chromatin remodeling such as DNA methylation, histone variants, covalent histone modifications, and ATP-dependent chromatin remodeling play important roles in carcinogenesis.[25,26] Indeed, poorly differentiated gastric adenocarcinoma is reported to lose Brm, a subunit of ATP-dependent chromatin-remodeling complex.[27] It can be assumed that these epigenetic changes lead to the chromatin-unfolding state and allow ready access to core histone protein. It might be also plausible that the higher cellular density of the poorly differentiated cancer tissues compared to other tissues explains the reason underlying the successful detection of a vast majority of histological type-specific signals from IMS. Conversely, signals specific to well- or moderately differentiated adenocarcinoma reflect the more-significant changes among the three histological types.

IMS technique was originally applied for the analysis of frozen tissue sections. FFPE samples are unsuitable for performing IMS due to the presence of cross-linkage between proteins and the inefficiency of enzyme digestion. Thus, few studies have reported the performance of IMS on FFPE samples.[28–30] Further, our study was hampered due to the disadvantage of FFPE. Due to the low S/N ratio, the identification of cancer- or histological type-specific proteins was rendered difficult.

TMA was originally used for IHC or *in situ* hybridization.[11,31] While this study was being conducted, another group reported the IMS of lung tumor biopsy in FFPE-TMA samples.[32] Thus, the FFPE-TMA-IMS has now emerged as the newest imaging technique. Other researchers have used this technique as an imaging tool to detect signals showing characteristic distribution in a particular tissue spot.[32] In contrast, we used the technique as a scanner for multiprocessing proteomics to readily detect cancer-specific signals. Two studies along these lines have reported highly different approaches. In this work, we loaded 12 tissue spots with 3-mm diameter in a TMA. Due to improvements in IMS resolution, the tissue spot size can now be reduced to submillimeter scales, enabling the loading of hundreds of tissue samples in one TMA. Thus, this technique can be applied for the analysis of a greater number of samples for high-throughput analysis of cancer characteristics.

Once a patient develops cancer, he or she should be subjected to medical treatments, including surgical operation and/or chemotherapy. To enable early detection of cancers, specific and sensitive biomarkers are desired. Using 2-DE based on MALDI mass spectrometry, potential proteins related to carcinogenesis have been discovered.[33,34] Further, in cases of far advanced or recurrent gastric carcinoma, chemotherapy prolongs the survival of the patient at a certain rate.[35] Proteomic analysis yielded an antidrug resistance agent,[36] while multidrug resistances were observed in certain cases. For retrospective evaluation and prospective searches of chemotherapy-related markers, high-throughput pathological evaluation methods are essential. IMS using TMA in FFPE, as we show here, will be one of the most promising gadgets in the surgical pathology laboratory.

In conclusion, we performed IMS of FFPE-TMA samples of gastric carcinoma, and successfully identified histone H4 as a signal specific to poorly differentiated cancer tissues. Moreover, the IMS-based finding was confirmed by IHC analyses of a large amount of TMAs. IMS of FFPE samples is a currently emerging

doi: 10.1111/j.1349-7006.2009.01384.x

technique and our experience represents an important step in the early phase of development. IMS of FFPE-TMA can offer fast and easy screening of cancer or tissue type-specific signals from a large amount of samples. The results of IMS-based screening can be readily verified by IHC analysis with other sets of FFPE-TMA samples. Combined with IHC confirmation, IMS of FFPE-TMA samples may be a further powerful tool in cancer proteomics.

Acknowledgments

This work was supported by a SENTAN step-up grant from JST to M.S. and by Grants-in-Aid from the Ministry of Health, Labour and Welfare for the Comprehensive 10-Year Strategy for Cancer Control (19-19) and the Third Term Comprehensive Control Research for Cancer; the Japan Society for the Promotion of Science for Scientific Research (no. 19790286), and the Smoking Research Foundation.

References

1 DeRisi J, Penland L, Brown PO *et al.* Use of a cDNA microarray to analyse gene expression patterns in human cancer. *Nat Genet* 1996 Dec; **14** (4): 457–60.
2 Ramsay G. DNA chips: state-of-the art. *Nat Biotechnol* 1998 Jan; **16** (1): 40–4.
3 Zhao X, Li C, Paez JG *et al.* An integrated view of copy number and allelic alterations in the cancer genome using single nucleotide polymorphism arrays. *Cancer Res* 2004 May 1; **64** (9): 3060–71.
4 Engle LJ, Simpson CL, Landers JE. Using high-throughput SNP technologies to study cancer. *Oncogene* 2006 Mar 13; **25** (11): 1594–601.
5 McLendon R, Friedman A, Bigner D *et al.* Comprehensive genomic characterization defines human glioblastoma genes and core pathways. *Nature* 2008 Oct 23; **455** (7216): 1061–8.
6 Ley TJ, Mardis ER, Ding L *et al.* DNA sequencing of a cytogenetically normal acute myeloid leukaemia genome. *Nature* 2008 Nov 6; **456** (7218): 66–72.
7 Hood L, Heath JR, Phelps ME, Lin B. Systems biology and new technologies enable predictive and preventative medicine. *Science* 2004 Oct 22; **306** (5696): 640–3.
8 Aebersold R, Mann M. Mass spectrometry-based proteomics. *Nature* 2003 Mar 13; **422** (6928): 198–207.
9 Diamandis EP. Mass spectrometry as a diagnostic and a cancer biomarker discovery tool: opportunities and potential limitations. *Mol Cell Proteomics* 2004 Apr; **3** (4): 367–78.
10 Sreekumar A, Nyati MK, Varambally S *et al.* Profiling of cancer cells using protein microarrays: discovery of novel radiation-regulated proteins. *Cancer Res* 2001 Oct 15; **61** (20): 7585–93.
11 Kononen J, Bubendorf L, Kallioniemi A *et al.* Tissue microarrays for high-throughput molecular profiling of tumor specimens. *Nat Med* 1998 Jul; **4** (7): 844–7.
12 Stoeckli M, Chaurand P, Hallahan DE, Caprioli RM. Imaging mass spectrometry: a new technology for the analysis of protein expression in mammalian tissues. *Nat Med* 2001 Apr; **7** (4): 493–6.
13 Shimma S, Sugiura Y, Hayasaka T, Zaima N, Matsumoto M, Setou M. Mass imaging and identification of biomolecules with MALDI-QIT-TOF-based system. *Anal Chem* 2008 Feb 1; **80** (3): 878–85.
14 Shimma S, Furuta M, Ichimura K, Yoshida Y, Setou M. Direct MS/MS analysis in mammalian tissue sections using MALDI-QIT-TOFMS and chemical inkjet technology. *Surf Interface Anal* 2006; **38** (2): 1712–14.
15 Groseclose MR, Andersson M, Hardesty WM, Caprioli RM. Identification of proteins directly from tissue: *in situ* tryptic digestions coupled with imaging mass spectrometry. *J Mass Spectrom* 2007 Feb; **42** (2): 254–62.
16 Crew KD, Neugut AI. Epidemiology of gastric cancer. *World J Gastroenterol* 2006 Jan 21; **12** (3): 354–62.
17 Japanese Gastric Cancer A. Japanese classification of gastric carcinoma – 2nd English edn. *Gastric Cancer* 1998 Dec; **1** (1): 10–24.
18 Schwartz SA, Reyzer ML, Caprioli RM. Direct tissue analysis using matrix-assisted laser desorption/ionization mass spectrometry: practical aspects of sample preparation. *J Mass Spectrom* 2003 Jul; **38** (7): 699–708.
19 Espada A, Rivera-Sagredo A. Ammonium hydrogencarbonate, an excellent buffer for the analysis of basic drugs by liquid chromatography-mass spectrometry at high pH. *J Chromatogr A* 2003 Feb 14; **987** (1–2): 211–20.
20 Wong JW, Cagney G, Cartwright HM. SpecAlign – processing and alignment of mass spectra datasets. *Bioinformatics* 2005 May 1; **21** (9): 2088–90.
21 Whistler T, Rollin D, Vernon SD. A method for improving SELDI-TOF mass spectrometry data quality. *Proteome Sci* 2007; **5**: 14.
22 Yanaga Y, Awai K, Nakaura T *et al.* Optimal contrast dose for depiction of hypervascular hepatocellular carcinoma at dynamic CT using 64-MDCT. *AJR Am J Roentgenol* 2008 Apr; **190** (4): 1003–9.
23 Lemaire R, Desmons A, Tabet JC, Day R, Salzet M, Fournier I. Direct analysis and MALDI imaging of formalin-fixed, paraffin-embedded tissue sections. *J Proteome Res* 2007 Apr; **6** (4): 1295–305.
24 Seeley EH, Caprioli RM. Molecular imaging of proteins in tissues by mass spectrometry. *Proc Natl Acad Sci USA* 2008 Nov 25; **105** (47): 18126–31.
25 Wang GG, Allis CD, Chi P. Chromatin remodeling and cancer, part I: covalent histone modifications. *Trends Mol Med* 2007 Sep; **13** (9): 363–72.
26 Wang GG, Allis CD, Chi P. Chromatin remodeling and cancer, part II: ATP-dependent chromatin remodeling. *Trends Mol Med* 2007 Sep; **13** (9): 373–80.
27 Yamamichi N, Inada K, Ichinose M *et al.* Frequent loss of Brm expression in gastric cancer correlates with histologic features and differentiation state. *Cancer Res* 2007 Nov 15; **67** (22): 10727–35.
28 Aoki Y, Toyama A, Shimada T *et al.* A novel method for analyzing formalin-fixed paraffin embedded (FFPE) tissue sections by mass spectrometry imaging. *Proc Jpn Acad Ser B* 2007; **83** (2): 205–14.
29 Stauber J, Lemaire R, Franck J *et al.* MALDI imaging of formalin-fixed paraffin-embedded tissues: application to model animals of Parkinson disease for biomarker hunting. *J Proteome Res* 2008 Mar; **7** (3): 969–78.
30 Ronci M, Bonanno E, Colantoni A *et al.* Protein unlocking procedures of formalin-fixed paraffin-embedded tissues: application to MALDI-TOF imaging MS investigations. *Proteomics* 2008 Sep; **8** (18): 3702–14.
31 Sugimura H. Detection of chromosome changes in pathology archives: an application of microwave-assisted fluorescence *in situ* hybridization to human carcinogenesis studies. *Carcinogenesis* 2008 Apr; **29** (4): 681–7.
32 Groseclose MR, Massion PP, Chaurand P, Caprioli RM. High-throughput proteomic analysis of formalin-fixed paraffin-embedded tissue microarrays using MALDI imaging mass spectrometry. *Proteomics* 2008 Sep; **8** (18): 3715–24.
33 Yoshihara T, Kadota Y, Yoshimura Y *et al.* Proteomic alteration in gastric adenocarcinomas from Japanese patients. *Mol Cancer* 2006; **5**: 75.
34 Cheng Y, Zhang J, Li Y, Wang Y, Gong J Proteome analysis of human gastric cardia adenocarcinoma by laser capture microdissection. *BMC Cancer* 2007; **7**: 191.
35 Ohtsu A. Chemotherapy for metastatic gastric cancer: past, present, and future. *J Gastroenterol* 2008; **43** (4): 256–64.
36 Wang X, Lu Y, Yang J *et al.* Identification of triosephosphate isomerase as an anti-drug resistance agent in human gastric cancer cells using functional proteomic analysis. *J Cancer Res Clin Oncol* 2008 Sep; **134** (9): 995–1003.

Supporting Information

Additional Supporting Information may be found in the online version of this article:

Fig. S1. The array images obtained with imaging mass spectrometry (IMS) are shown. There are 18 evenly distributed images and 37 cancer specific ones, two well-differentiated adenocarcinoma-specific images, one well- and moderately differentiated adenocarcinoma-specific image, two moderately differentiated adenocarcinoma-specific images, four moderately and poorly differentiated adenocarcinoma-specific images, and eight poorly differentiated adenocarcinoma-specific images. Values are represented as mean ± SD ($n = 3$). $^*P < 0.05$. $\dagger P < 0.05$.

Please note: Wiley-Blackwell are not responsible for the content or functionality of any supporting materials supplied by the authors. Any queries (other than missing material) should be directed to the corresponding author for the article.

Secreted form of *EphA7* in lung cancer

MASARU TSUBOI[1], HIROKI MORI[1], TOMOYASU BUNAI[1], SHINJI KAGEYAMA[1], MASAYA SUZUKI[1], KOJI OKUDELA[1], KAZUYA TAKAMOCHI[2], HIROSHI OGAWA[3], HIROSHI NIWA[4], KAZUYA SHINMURA[1] and HARUHIKO SUGIMURA[1]

Departments of [1]Pathology and [2]Respiratory Surgery, Hamamatsu University School of Medicine, 1-20-1 Handayama, Higashi-ward, Hamamatsu 431-3192; Departments of [3]Pathology and [4]Respiratory Surgery, Seirei Mikatahara Hospital, 3453 Mikataharacho, Kita-ward, Hamamatsu 423-8558, Japan

Received September 25, 2009; Accepted November 18, 2009

DOI: 10.3892/ijo_00000539

Abstract. EPHA7 is a member of the EPHA family of receptor kinases, among which several members are known to be involved in human lung carcinogenesis. We report here a novel spliced variant, the so-called secreted form of EPHA7, recently reported in malignant lymphoma, in human lung cancer cell lines and primary lung cancer. In contrast to the *EPHA7* down-regulation in colorectal cancer by promoter hypermethylation, EPHA7 is expressed at a substantial level in most human lung cancers and the secreted form of EPHA7 mRNA was found in a fraction of primary lung cancer tissues, lung cancer cell lines, and immortalized bronchogenic epithelial cell lines. Interestingly, the secreted form of *EPHA7* message was predominantly detected in non-adeno type lung carcinoma. The mechanistic role of the secreted form of *EPHA7* in human lung carcinogenesis is not clear, but the presence of this form could distinctly exclude adenocarcinoma of the lung from the other categories, i.e., squamous cell carcinoma, small cell carcinoma and large cell carcinoma, which have strong association with smoking. This is the first study to detect the secreted form of *EPHA7* in human epithelial tissues. EPHA7 warrants further investigation to determine its possible involvement in smoking related lung carcinogenesis.

Introduction

The erythropoietin producing hepatocellular carcinoma (EPH) family of receptor tyrosine kinases constitutes the RTK subfamily and members of this family are divided into EPHAs and EPHBs. EPHAs are typically bound to Ephrin(EFN)As, which are anchored to the cell membrane via a glycosylphosphatidylinositol anchor. EPHBs are typically bound to EFNBs, which have a transmenbrane domain (1). These molecules take bidirectional signal pathways, EFN to EPH forward signal and EPH to EFN reverse signal, and these pathways are involved in many physiological and pathological conditions (2). Members of this family play critical roles in many facets of cancer biology, from initiation to metastasis and also invasion (3-6). Almost all the human cancers have been reported to be associated with some of the EPH-EFN pathways (7-11). EPHA family genes, especially *EPHA3* and *EPHA5*, are among the genes which often mutate in human lung cancer, as demonstrated by a recent extensive large scale coding sequence analysis (12). EPHA7 is a member of the EPHA family, but it has been investigated in only a few human lung cancers. The recent finding of its downregulation by promoter methylation and a possible tumor suppressing effect in several types of human cancer (8,13,14) prompted us to investigate the expression status of EPHA7 in human lung cancer, to assess the possibility of a tumor suppressor role in lung carcinogenesis. On the other hand, the locus of *EPHA7* is near the breakpoint of t(3;6) in renal cell carcinoma (15). Considering the recent discovery of various translocations in solid tumors (16,17), especially in lung carcinoma (18-20), we also anticipated translocation involving this gene locus in lung cancer.

Materials and methods

Cell lines. Forty cell lines, consisting of 3 normal lung cells (SAEC, 16HBET14o- and WI-38), 10 lung adenocarcinomas (H358, H820, H2087, A549, HLC-1, RERF-LC-MS, RERF-LC-KJ, LC-2/ad, VMRC-LCD and PC-3), one lung squamous cell carcinoma (ABC-1), four lung large cell carcinomas (H460, H1299, LU65 and PC-13), five lung small cell carcinomas (H526, H1688, TKB-2, Lu-130 and Lu-135), three colon adenocarcinomas (HCT116, HT29 and DLD-1), eight gastric adenocarcinomas (AGS, HSC-39, KATO3, MKN-1, MKN-28, MKN-45, MKN-74 and TMK-1) and four esophageal squamous cell carcinomas (A431, HSC-2, HSC-3 and HSC-4), were used in this study. The 16HBE14o- cell line (Simian virus 40-transformed human bronchial epithelial cells) was a gift from Dr D.C. Gruenert (California Pacific Medical Center Research Institute, San Francisco, CA, USA) via Dr T. Kaneko (Department of Internal Medicine, Yokohama City University, School of Medicine, Yokohama,

Correspondence to: Dr Haruhiko Sugimura, First Department of Pathology, Hamamatsu University School of Medicine, 1-20-1 Handayama, Higashi-ward, Hamamatsu 431-3192, Japan
E-mail: hsugimur@hama-med.ac.jp

Key words: EPHA7, lung cancer

Japan) (21). The Lu-130, Lu-135 and PC-13 cell lines were gifts from Dr Y. Dobashi (Jichi Medical University, Omiya Medical Center Hospital, Omiya, Japan). A549, ABC-1, H460, LC-2/ad, VMRC-LCD, RERF-LC-MS, REAF-LCKJ and TKB-2 were gifts from Dr T. Niki (Jichi Medical University, Shimotsuke, Japan). TMK-1 was a gift from the Department of Genetics, National Cancer Center (Tokyo, Japan). SAEC was purchased from Clontech (San Diego, CA). WI-38, H358, H820, H2087, H1299, H526, H1688, HCT116, HT-29, DLD-1 and AGS were obtained from ATCC (Manassas, VA, USA). PC-3, LU65, KATO3, MKN-1, MKN-28, MKN-45, MKN-74, A431, HSC-2, HSC-3 and HSC-4 were obtained from the Health Science Research Resources Bank (Osaka, Japan). HLC-1 was obtained from RIKEN Cell Bank (Ibaraki, Japan).

Clinical samples. The subjects were selected from among patients of Hamamatsu University School of Medicine and Mikatahara Seirei General Hospital. Written informed consent to participate in this study was obtained and the entire study design was approved by the Institutional Review Boards (IRB) of Hamamatsu University School of Medicine (18-4,18-5) and Mikatahara Seirei General Hospital. Lifestyle information such as smoking habits was obtained by professional interviewers. Histopathological classification was performed according to the WHO classification (2004) (22). Stages of the clinical samples according to the TNM classification system (http://www.uicc.org/) are shown in Table I.

3'-Rapid amplification of cDNA end. 3'-RACE was performed with the 3' RACE System for Rapid Amplification of cDNA Ends (Invitrogen). Briefly, the first strand cDNA was reverse transcribed from 1 μg of total RNA using SuperScript II RT (Invitrogen) and the adapter primer; 1 μl of the first strand cDNA was then amplified using an *EPHA7* gene-specific forward primer (EphA7 RACE 5'-CACCATACGTTGCATG CACA-3') and the Universal Amplification Primer. In the polymerase chain reactions, after initial denaturation at 95˚C for 15 min, 35 cycles of denaturation at 95˚C for 30 sec, annealing at 58˚C for 30 sec, and elongation at 72˚C for 45 sec were used, followed by a final elongation step at 72˚C for 5 min.

Sequencing of the RACE product and validating sequencing of the secreted form of EPHA7 (EPHA7-S). We sequenced the band of ~600 bp generated by the RACE procedure with an *EPHA7* gene-specific forward sequencing primer, and identified it as *EPHA7*-S. We searched for EPHA7-S in lung cancer cell lines by sequencing the cDNAs synthesized from mRNAs. Gene-specific primer pairs were designed to cover the region from exon 4 to intron 5 of *EPHA7*. Primers for PCR were 5'-CATCTGACCCACCATACGTTGC-3' (*EPHA7* exon 4) and 5'-GCTGGAAGAATCAAGCTCTGTG-3' (*EPHA7* intron 5). PCR was carried out in reaction mixtures containing cDNA, 1X HotStar Taq buffer, 0.25 mmol/l deoxynucleotide triphosphate mixture, 0.05 U of HotStar Taq (Qiagen, Dusseldorf, Germany), and 0.5 mmol/l of forward and reverse primers in a volume of 20 μl. PCR cycling parameters were one cycle of 95˚C for 15 min; 40 cycles of 95˚C for 30 sec, 58˚C for 30 sec, and 75˚C for 45 sec; followed by one cycle of 72˚C for 5 min. The PCR products were purified with a PCR purification kit (Qiagen) and directly sequenced with a Big Dye Terminator Cycle Sequencing Reaction Kit and the ABI 3100 Genetic Analyzer (Applied Biosystems Incorporated, Tokyo, Japan). Sequencing reactions were done in both forward and reverse directions with two primers for PCR.

Table I. Clinicopathological characteristics of the patients.

No of patients, N	73
Average age (range), years	64.7 (39-83)
Gender, n (%)	
Male	41 (56.2)
Female	32 (43.8)
Histology, n (%)	
Adenocarcinoma	50 (68.3)
Squamous cell carcinoma	17 (23.3)
Small cell carcinoma	2 (2.7)
Large cell carcinoma	4 (5.5)
Brinkman index, n (%)	
BI = 0	24 (32.9)
0<BI≤400	4 (5.5)
400<BI	36 (49.3)
Unknown	9 (12.3)
TNM stage, n (%)	
I	47 (64.4)
II	6 (8.2)
III	13 (17.8)
IV	3 (4.1)
Unknown	4 (5.5)

Statistical analysis. χ^2 analysis and the Cochran-Armitage trend test were conducted to compare EPHA7-S expression with various clinical features (sex, smoking history, histological type, and TNM stages). A $p<0.05$ was considered significant. Statistical analyses were performed using the SAS (Statistical Analysis System) program (SAS Institute Japan, Tokyo, Japan).

Results

Detection of EPHA7-S in cell lines. First, we attempted to identify a downstream sequence, expecting a fusion partner of EPHA7. We adopted the 3'-RACE method using the primer corresponding to exon 4 of *EPHA7* and the RACE specific 3' primer for the RNAs from PC-13 and H82 cell lines, both of which express EPHA7 (data not shown). The RERF-LC-MS cell line, which has no EPHA7 expression, was used as a negative control. By the 3'-RACE method, we detected amplified fragments in both PC-13 and H82 (Fig. 1a).

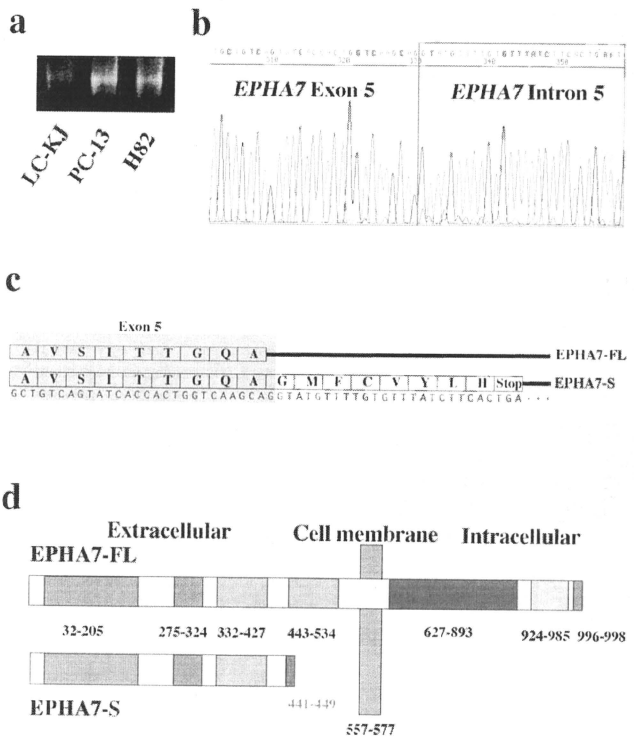

Figure 1. Detection of the secreted form of EPHA7 (EPHA7-S) in lung cancer cell lines. (a) 3'-RACE method showing amplification of EPHA7-S in PC-13 and H82 but not in RERF-LC-KJ. (b) Sequencing analysis of the EPHA7-S gene transcript of PC-13. The red box indicates intron 5 of the *EPHA7* gene. (c) Nucleotide sequence and predicted amino acid sequence of full-length EPHA7 (EPHA7-FL) at the end of exon 5 and for the EPHA7-S based on sequencing of a cDNA from the PC-13 cell line. Shaded region is exon 5 of the *EPHA7* gene. (d) Schematic representation of EPHA7-FL and EPHA7-S. 32-205, Ephrin receptor ligand binding domain; 275-324, TNF receptor domain; 332-427 and 443-534, Fibronectin type 3 domain; 557-577, transmenbrane domain; 627-893, tyrosine kinase domain; 924-985, SAM domain; 996-998, PDZ binding motif; 441-449, intron 5 (EPHA7-S).

Sequencing analysis of these fragments disclosed that they were not fusion partners, while the sequence derived from EPHA7 itself had its intron 5 (Fig. 1b and c). DNase treatment and the cDNA minus negative control excluded the possibility of mis-amplification of the genomic sequence. This cDNA contained the exon 5 sequence directed to the intron 5 sequence of *EPHA7* (Fig. 1c), and it had a stop codon after coding 8 amino acids, generating the structure lacking the transmembrane domain of the authentic EPHA7 (Fig. 1d). Given these structural features, we consider this form to be the human counterpart of EphA7-S reported in murine lymphocytes by Dawson *et al* (23). In addition, they demonstrated human tonsillar lymphocytes to also express an EPHA7-S protein of consistent size by Western blotting, though the exact message was not shown (23). This structure lacks a cytoplasmic domain, which would include a kinase domain, indicating that the product would be secreted outside the cells.

EPHA7-S expression in lung cell lines. We examined cell lines, including those of lung cancers, gastrointestinal cancers and immortalized bronchial epithelium, for detection of EPHA7-S. We used the primers in the *EPHA7* exon 4 (forward) and intron 5 (reverse) for reverse transcription PCR. This primer set discriminates the contaminated genomic amplified product (1677 bp) from the target product (475 bp) (Fig. 2a). EPHA7-S was detected mainly in lung cancer cell lines, rarely in those from other organs (16/21 in lung cancer cell lines vs. 1/15 gastrointestinal cancer cell lines) (Fig. 2b and Table II). that is, EPHA7-S is a variant occurring mainly in lung cancer cells.

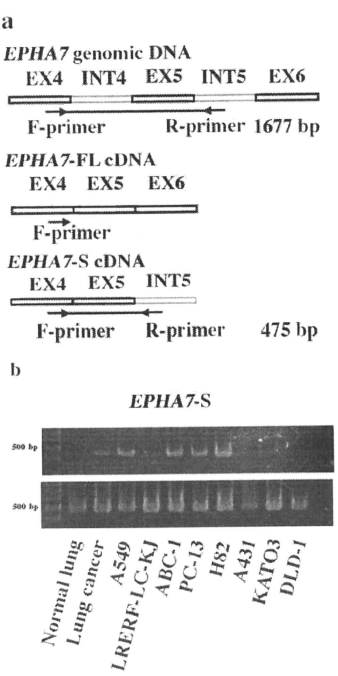

Figure 2. Secreted form of EPHA7 (EPHA7-S) in various cell lines. (a) PCR primer design and the structure of EPHA7-S. The amplified structure of genomic *EPHA7* (1677 bp) is shown above, EPHA7-FL cDNA (no amplification) is the middle, and EPHA7-S cDNA (475 bp) below. (b) EPHA7-S cDNA (475 bp) was detected in some of these cell lines. The bands in the upper panel are EPHA7-S and those in the lower panel sare GAPDH. The sources of the normal lung and lung cancer lanes are clinical samples from patient no. 15 (squamous cell carcinoma and the corresponding non-tumor lung portion). A549, LRERF-LC-KJ, ABC-1, PC-13 and H82 are lung cancer cell lines. A431 is an esophageal cancer cell line, KATO3 is a gastric cancer cell line, and DLD-1 is a colon cancer cell line. The left-most lane indicates size markers, a 100-bp DNA ladder.

Some clinical lung cancer specimens express EPHA7-S. The tendency for EPHA7 to be expressed by lung cancer cell lines prompted us to look for it in primary lung cancer tissues. A substantial proportion of human primary lung cancers expressed EPHA7-S; 2 out of 50 cases with lung adenocarcinoma and 8 of 23 cases with non-adenocarcinoma of the lung. Among the non-adenocarcinoma cases, 6 of 17 squamous cell carcinoma cases, one of the two cases with small cell carcinoma, and one of four large cell carcinoma cases were positive for EPHA7-S (Table III). In 2 cases, EPHA7-S was detected in non-tumor lung tissue adjacent to the lung cancer (data not shown).

The prevalence of EPHA7-S was significantly greater in non-adenocarcinoma than in adenocarcinoma (Table IV). No

Table II. Secreted form of *EPHA7* (*EPHA7-S*) in various cell lines.

Material		EphA7-S
16HBE14o-	Normal human bronchial epithelium	+
SAEC	Small airway epithelial	+
WI-38	Lung fibroblast	-
H358	Lung adenocarcinoma	+
H820	Lung adenocarcinoma	+
H2087	Lung adenocarcinoma	-
A549	Lung adenocarcinoma	+
HLC-1	Lung adenocarcinoma	+
RERF-LC-MS	Lung adenocarcinoma	+
LC-2/ad	Lung adenocarcinoma	-
VMRC-LCD	Lung adenocarcinoma	+
PC-3	Lung adenocarcinoma	+
RERF-LC-KJ	Lung adenocarcinoma	-
ABC-1	Lung squamous cell carcinoma	+
H460	Lung large cell carcinoma	-
H1299	Lung large cell carcinoma	+
LU65	Lung large cell carcinoma	+
PC-13	Lung large cell carcinoma	+
H82	Lung small cell carcinoma	+
H526	Lung small cell carcinoma	+
H1688	Lung small cell carcinoma	+
Lu-130	Lung small cell carcinoma	+
Lu-135	Lung small cell carcinoma	+
TKB-2	Lung small cell carcinoma	-
DLD-1	Colon adenocarcinoma	-
HCT-116	Colon adenocarcinoma	-
HT29	Colon adenocarcinoma	-
AGS	Gastric adenocarcinoma	-
HSC-39	Gastric adenocarcinoma	+
KATO3	Gastric adenocarcinoma	-
MKN-1	Gastric adenocarcinoma	-
MKN28	Gastric adenocarcinoma	-
MKN-45	Gastric adenocarcinoma	-
MKN-74	Gastric adenocarcinoma	-
TMK-1	Gastric adenocarcinoma	-
A431	Esophageal squamous cell carcinoma	-
HSC-2	Esophageal squamous cell carcinoma	-
HSC-3	Esophageal squamous cell carcinoma	-
HSC-4	Esophageal squamous cell carcinoma	-

+, EPHA7-S detectable, -, not detectable.